


12-31-2010

Continuous Electrowetting Actuation Utilizing Current Rectification Properties of Valve Metal Films

Corey Lynch
University of South Florida

Follow this and additional works at: <http://scholarcommons.usf.edu/etd>

 Part of the [American Studies Commons](#), and the [Mechanical Engineering Commons](#)

Scholar Commons Citation

Lynch, Corey, "Continuous Electrowetting Actuation Utilizing Current Rectification Properties of Valve Metal Films" (2010).
Graduate Theses and Dissertations.
<http://scholarcommons.usf.edu/etd/3519>

This Thesis is brought to you for free and open access by the Graduate School at Scholar Commons. It has been accepted for inclusion in Graduate Theses and Dissertations by an authorized administrator of Scholar Commons. For more information, please contact scholarcommons@usf.edu.

Continuous Electrowetting Actuation Utilizing Current Rectification Properties
of Valve Metal Films

by

Corey M. Lynch

A thesis submitted in partial fulfillment
of the requirements for the degree of
Master of Science in Mechanical Engineering
Department of Mechanical Engineering
College of Engineering
University of South Florida

Major Professor: Nathan B. Crane, Ph.D.
Rasim Guldiken, Ph.D.
Craig Lusk, Ph.D.

Date of Approval:
October 22, 2010

Keywords: EWOD, Lab-on-a-chip, Digital Microfluidics,
MEMS, Fluidic Actuation

© Copyright 2010, Corey M. Lynch

Table of Contents

List of Tables	iii
List of Figures	iv
Abstract	v
Chapter 1. Introduction	1
1.1 Thesis Statement	1
1.2 Fundamentals of Electrowetting	2
1.3 Significance of Electrowetting	3
1.3.1 Micro- and Nano- Scale Engineering	3
1.3.2 Current/Near-Future Applications of Electrowetting	4
1.3.2.1 Display Technology	4
1.3.2.2 Microlenses and Fiber Optics	5
1.3.2.3 Lab on a Chip and Digital Microfluidics	6
1.3.3 Possible Future Applications of Electrowetting	9
1.4 Research Focus	10
Chapter 2. Literature Review and Basic Device Concepts	12
2.1 Previous Work	12
2.2 Governing Equations	14
2.3 Electrical Models	16
2.3.1 Grounded Droplet Electrical Configuration	16
2.3.2 Novel Actuation Concept	18
2.4 Creation of Diode Sites	22
2.4.1 Current Rectification in Valve Metals	23
2.4.2 Alternatives for Diode Creation	26
Chapter 3. Device Design	28
3.1 Device Modeling	28
3.1.1 Identification of Key Parameters	29
3.1.2 Define Parameter Interrelationships	33
3.2 Device Design	35

3.2.1 Components.....	36
3.2.1.1 Electrode	37
3.2.1.2 Dielectric Layer.....	38
3.2.1.3 Valve Metal.....	38
3.2.1.4 Surface Treatment.....	39
3.2.2 Fabrication Techniques	42
Chapter 4. Device Testing	49
4.1 Experimental Variables	49
4.2 Testing Setup.....	51
4.2.1 Equipment	51
4.2.2 Testing Procedure	54
4.3 Results.....	55
4.3.1 Minimum Actuation Voltage.....	60
4.3.2 Droplet Velocity	62
4.3.3 Further Testing.....	64
4.3.4 Analysis.....	65
Chapter 5. Conclusion	71
5.1 Summary	71
5.2 Future Work	73
List of References.....	76
Appendices.....	80
Appendix A. Modified C++ Code for Camera Trigger Software	81

List of Tables

Table 1. Equivalent electrical components	37
Table 2. Standard-thickness CYTOP spin-coat program.....	45
Table 3. Reduced-thickness CYTOP spin-coat program	45
Table 4. Wafer layer dimensions	47
Table 5. Strip/Site dimensions	47
Table 6. Results for minimum actuation voltage on Wafer 4	62
Table 7. Results for droplet velocity on Wafer 4.	63
Table 8. Testing results for 1M Na ₂ SO ₄ under hexadecane	64
Table 9. <i>P</i> -values from ANOVA performed on minimum actuation voltage data.....	68
Table 10. <i>P</i> -values from ANOVA performed on droplet velocity data	70

List of Figures

Figure 1. Multi-electrode asymmetric electrowetting.....	8
Figure 2. Schematic representation of Young's equation.	15
Figure 3. Idealized equivalent circuit of current EWOD designs for droplet transport.....	17
Figure 4. Idealized equivalent circuit of proposed EWOD device	19
Figure 5. Array of diode-capacitor sites demonstrating how continuous motion is achieved.	22
Figure 6. Current-Voltage plot of aluminum illustrating current rectifying property.....	26
Figure 7. Construction techniques for electrowetting device.	42
Figure 8. Wafer pattern schematic.....	46
Figure 9. Generic test strip diagram.	48
Figure 10. Testing equipment schematic.....	53
Figure 11. Photocompilation of successful test run.	57
Figure 12. Current-Voltage plot for Wafer 1 and Wafer 2 dielectric layer.	58
Figure 13. Current-Voltage plot of aluminum site on Wafer 3.....	59
Figure 14. Photograph illustrating teardrop shape of electrolyte droplet with 3-wide site configuration.....	69

Abstract

Electrowetting on dielectric (EWOD) is a technique for reducing the apparent contact angle of a fluid droplet, which has many promising applications in the fields of optics, digital displays, and lab-on-a-chip research. In this thesis, a design is presented for a novel single circuit device for achieving continuous droplet motion, by using the current-rectifying properties of valve metals to create diode-like behavior. This contrasts with existing designs, which require an array of individual electrodes to achieve motion in discrete steps. We are able to demonstrate continuous droplet motion across a 28mm-long test strip with an applied voltage of 303 V and a velocity of 5.59 mm/s (at 370 V) using an ionic-fluid electrolyte (BMIM-PF6), and have achieved actuation at as low as 185 V, with a maximum observed velocity (at 300 V) of 13.8 mm/s using a 1M sodium sulfate solution.

Chapter 1.

Introduction

1.1 Thesis Statement

This thesis explores novel techniques in micro-droplet handling utilizing electrowetting on dielectric phenomena; specifically, the continuous movement of a droplet by geometrically asymmetric electrowetting. This contrasts with discrete droplet movement which has previously been achieved by asymmetric electrowetting has. Discrete droplet movement uses successive activation of an array of discrete small electrodes, several of which are covered by the drop. As each electrode is activated and the contact angle above it is reduced, the droplet is 'handed off' from electrode to electrode. This accomplishes droplet movement in successive discrete steps each having a magnitude equivalent to the size of the electrodes, while requiring somewhat complex control systems to control the activation of electrodes in the proper sequence and with the proper timing.

In contrast, the approach discussed in this thesis allows for smooth continuous droplet movement across what is essentially a single circuit using a continuous DC voltage. This is achieved by taking advantage of the current-rectifying properties of oxide films on the so-called valve metals. By patterning an array of holes in the dielectric layer, under which lies a valve metal electrode,

and applying a potential across the electrode, the side of the droplet above the anodic hole will have its contact angle reduced. As the droplet flows to cover the next-most-positively charged hole, the previously anodic hole will become cathodic (allowing current flow) and the newly-covered hole will become anodic, causing the contact angle to be reduced over it. This sequence is repeated until the potential is removed or the array of holes ends.

1.2 Fundamentals of Electrowetting

Electrowetting can be defined as the phenomenon whereby the application of a difference in electric potential (voltage) between a solid electrode and a small droplet of a non- or partially-wetting conductive fluid (lying on the electrode) results in a decrease in the apparent contact angle between droplet and substrate, effectively increasing the wettability of the interface [1]. For almost 100 years, those studying this phenomenon used the same architecture as the first man to do so (Gabriel Lippmann), namely an electrode (often mercury) in direct contact with an electrolyte. This introduced limitations due to electrolytic decomposition of water at anything higher than minimal voltages (hundreds of millivolts).

In more recent years, this problem has been eliminated by the introduction of a thin dielectric (insulating) layer between the electrode and electrolyte, which has the effect of dramatically increasing the allowed voltage. This architecture (with either air, inert gas, or often an insulating oil as the third 'ambient' phase)

has formed the basis for most recent research into the area and has been termed Electrowetting on Dielectric [1]. There have been several approaches taken by different researchers in describing the mechanism responsible for electrowetting but the fundamental premise is that the application of a difference in electrical potential (voltage) causes charge migration within the droplet and the electrode. By altering the surface energies of the interface, this causes a change in the effective surface tension between the droplet and substrate. At the small scales under examination, capillary forces and surface tensions are the primary determiners of droplet behavior and so alteration of these forces cause significant changes in droplet geometry. The net effect is that this modification of the effective surface tension at the three phase contact line causes a reduction in apparent contact angle between the droplet and the substrate, increasing the wettability of the interface [1][2].

1.3 Significance of Electrowetting

1.3.1 Micro- and Nano- Scale Engineering

Recent years have seen a dramatic increase in the study of micro- and nano-scale structures, systems, and manufacturing techniques. While the benefits of such advances are obvious for many applications due simply to the small sizes involved (less invasive medical devices, smaller electronic components, etc.), other less immediately obvious benefits exist. The efficiency

of many devices can be increased dramatically by their construction on such small scales.

Additionally, these scales allow for assembly and manufacturing techniques that can drastically improve the speed and quality of the process, and which would not be possible on more typical size scales. While it has significant benefits, working on such a small scale comes with difficulties. The dramatic increase in surface area-to-volume/mass ratios means that surface energies and other interfacial effects play a much more significant role in interactions between parts and substances [3, 4]. While this results in many of the benefits discussed above (e.g. self assembly techniques), it also means that many of the assumptions and simplifications commonly made in more typical bulk-scale engineering analyses are invalid. As more and more applications for nano-scale devices and techniques are being discovered, a more complete understanding of the behavior of these systems is needed. As such, the study of any unexplored property or phenomenon of micro- or nano-scale devices (such as electrowetting techniques) has significant value.

1.3.2 Current/Near-Future Applications of Electrowetting

1.3.2.1 Display Technology

The practical applications of EWOD are diverse. One of the areas in which commercial applications are already being brought to market is in the field of display technology. By combining small amounts of a dyed naturally wetting oil

and transparent naturally non-wetting electrolyte into a small pixel, a simple monochromatic display can be created. The application of voltage to the pixel causes the transparent electrolyte to wet the electrode, displacing the oil layer and causing it to retract (often to a corner which has previously been treated to be a preferential location for the oil to wet). When voltage is removed the oil film re-spreads to cover the pixel, making it 'dark' again. By combining clusters or layers of small pixels of several different colors a multicolor display is achievable. Pixel-switching times are fast enough to support video displays using this technique[5]. The advantages of such a system over current video displays are many-fold. The root of several of these benefits is the lack of a backlight (as is necessary for LCDs and other current technologies) since ambient light reflected off the display is all that is needed to discern the image. The most significant benefit for the small-electronics market is their dramatically reduced power consumption as compared to existing LCD technology. Additionally, this lack of a backlight leads to better visibility under bright ambient-light conditions (full sunshine) and reduced eye fatigue [6] [7-9].

1.3.2.2 Microlenses and Fiber Optics

Another application with lucrative commercial potential is in the field of microlenses. The droplet in an electrolyte-oil system can be used as a lens in small-scale optics (e.g. cell-phone cameras, sensing devices) where the ability to change focal length 'on-the-fly' without moving parts is desirable. By varying the

voltage applied to the droplet, it is possible to cause changes in the shape of the droplet, thereby changing its optical properties [10]. Alternatively, electrowetting techniques can be used in the manufacture of solid microlenses. The shape of a droplet of liquid photopolymer can be manipulated through electrowetting. When the desired optical properties have been achieved the photopolymer can then be cured via light exposure to produce small solid lenses [1]. In the field of fiber optics, several designs have been proposed for signal modification through the use of electrowetting. By selectively moving (by electrowetting) an electrolyte droplet with a specific refractive index to either cover or uncover a section of fiber optic cable with its coating stripped, both narrow and broad band attenuation of the signal can be achieved [11].

1.3.2.3 Lab on a Chip and Digital Microfluidics

One application seeing intense development is the 'Lab-on-a-Chip' concept. The end goal of these efforts is to create a micro electromechanical system (MEMS) device which will perform tests/analyses previously requiring a laboratory. The advantages of such a device (over a traditional laboratory) are diverse [12, 13]. Many are the result of the reduced volume of fluid needed for tests performed on such a small scale. This means less must be spent on reagents, and less of the sample is needed. Additionally, due to the reduced diffusion distances, process times are reduced, and the processes can typically be controlled more easily (the reduced mass eliminates the 'damping' effect in

response to heating, etc.). The reduction in fluid volume can also increase the safety of the test when chemically, biologically or radioactively hazardous materials are a component of the test. In addition to these benefits, the architecture used as the structural basis of these devices is an extremely developed science (due to its use in the semiconductor industry) meaning low-cost mass production is possible [14].

At the core of these lab-on-a-chip designs is the science of microfluidics. In contrast to continuous-flow micro-fluidics, which (as its name suggests) deals with control of steady flows of fluid, digital micro-fluidics focuses on the manipulation of discrete droplets of fluids. These droplets can be separated from a reservoir, transported, cut, merged, and mixed to perform various tests[15-17]. Electrowetting on dielectric techniques have been used to achieve these goals by several groups. As mentioned previously, the current architecture has been to use several electrodes, each small enough that the droplet being manipulated will straddle at least 2-3 electrodes at any point. By selectively activating only one of the electrodes under a droplet, it is possible to asymmetrically 'electrowet'. In such a situation, the contact angle is reduced only on one side of the droplet, causing the droplet to flow in that direction, as shown in Figure 1 [18, 19].

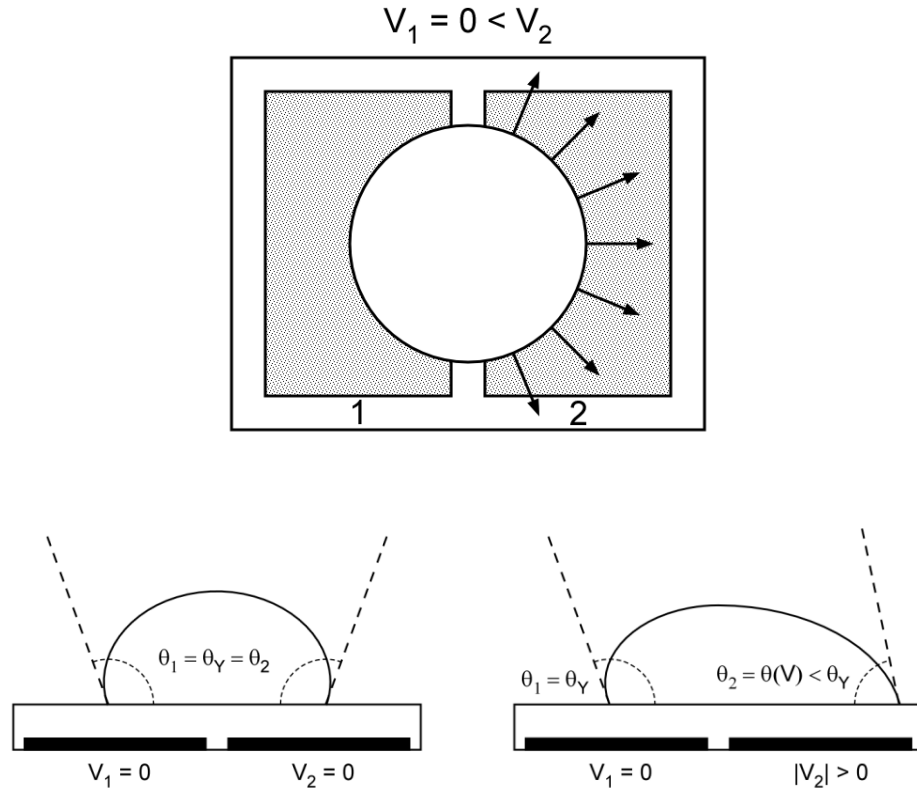


Figure 1. Multi-electrode asymmetric electrowetting. (Upper) Top view, Arrows indicate the forces acting on the three-phase contact line. (Lower left) Side view, shows the natural (or Young's) contact angle when no voltage is applied. (Lower Right) Side view, shows the reduced contact angle (and resulting droplet asymmetry) when voltage is applied only to the right-hand electrode.

By activating individual electrodes in series, it is possible to “hand off” the droplet from one electrode to another, and move it across the chip. Similarly, by activating electrodes on opposite sides of a drop, it is possible to split it in two. Merging two drops is as simple as bringing them together [19, 20]. To mix the contents of a drop (after merging drops of two reactants perhaps) voltage can be

applied symmetrically (so that no translation occurs), but in an oscillatory manner, so that the contact angle is reduced, then returned to its natural state, several times in succession. This has the effect of effectively mixing the drop [17, 21]. While these techniques show much promise, they have the problem of being difficult to manufacture due to having several small electrodes and requiring several layers to accommodate the multitude of crossing electrical lines. Furthermore, they require complicated control systems (to activate the specific electrodes needed in the correct sequence and with the correct timing).

1.3.3 Possible Future Applications of Electrowetting

As more and more study is devoted to electrowetting on dielectric, novel and exciting applications are being theorized and developed. While many of these exist only as on-paper theories or relatively simple proof-of-concept prototypes, they open up new avenues of research and development, as well as serving as inspiration for the next group of researchers. One of the more interesting applications for EWOD being explored is as a means of propulsion, specifically for a water surface craft. Several teams using different techniques have constructed and tested proof-of-concept 'pond-skater' MEMS devices whose method of propulsion is based on electrowetting on dielectric. One uses a low frequency alternating-current voltage to produce periodic movement of the contact line between a floating 'chip' and the water which results in a net propulsive force [22]. Another captures bubbles under the surface of their 'boat'

and uses electrowetting techniques to eject the bubbles out one side, with the reaction force of this ejection providing propulsion. Interestingly, the second team, using novel construction techniques, was able to produce significant contact angle reduction with as low as 15V applied voltage, allowing them to power their device wirelessly using an RF signal [23].

Another application for electrowetting that has been proposed recently is in the construction of an electric motor. In this application a droplet of electrolyte is placed atop a circular array of several electrodes such that they lie under the circumferential edge of the droplet. Atop this droplet is placed a small floating plate with evenly spaced radial protuberances. When electrodes with the same angular spacing as the plate's protuberances are activated, they cause local reduction in the droplet's contact angle, resulting in an irregular droplet shape. In order to reach an equilibrium state, the floating plate will rotate until its protuberances align with the activated electrodes (minimizing droplet surface area). By next activating the electrodes to one side of each of the previously activated electrodes, and then continuing this process, steady rotation of the plate can be achieved. Prototypes of such motors have been able to achieve angular velocities of 180 rpm [24].

1.4 Research Focus

While the study of electrowetting on dielectric has seen significant progress in the past decades, there still remain unexplored avenues of research

and undiscovered applications. This paper focuses on one such new development. The current rectifying properties of oxide films on the so-called valve metals (those which readily form stable continuous oxide layers under standard atmospheric conditions) has long been known, and is in fact the source of their name [25]. By taking advantage of this property, it was theorized that a novel method of achieving droplet movement was possible. By reducing the design to essentially one circuit, and enabling the droplet to move continuously in the direction of potential difference, the complexity of the device as a whole would be dramatically reduced. Its control systems would be simpler, and the manufacturing less complex. In the following pages a brief introduction to electrowetting is given, and the basic governing principles are discussed. Following this, the current-rectification properties of valve metals are introduced, and the way in which they are incorporated into our device is detailed. A predictive model of device performance is discussed, along with its usefulness in designing our prototype device. The designs for our prototype design and subsequent improved versions are presented. The testing procedures used to evaluate our designs are presented, and the results of the tests are given and analyzed. Lastly, a summary of the work is given, and areas of emphasis for future work in this field are described.

Chapter 2.

Literature Review and Basic Device Concepts

In this chapter, a background in the field of electrowetting research is presented. First, an introduction is given to some of the more significant historical work done, which established the fundamentals of the field. Following this, the basic physical principles at work are explained, as well as the equations that arise from them which govern electrowetting behavior. Next, idealized electrical models of EWOD droplet transport devices are presented, illustrating the conceptual differences between current multi-electrode grounded droplet designs and the novel design being presented in this thesis. Lastly, a background on current rectification in valve metals is given, and their use in our proposed design is detailed.

2.1 Previous Work

The first person to discover the phenomenon which underlies electrowetting was Gabriel Lippmann in 1875 [2]. He discovered that the capillary depression of mercury which was in contact with an electrolytic solution could be modified by the application of an electrical potential difference across the mercury-electrolyte interface. He proceeded to develop a theoretical

framework to explain this behavior, as well as design several interesting applications for this new phenomenon, including an electrometer and even a motor. While study of the phenomenon continued, it was relatively stagnant and remained more of an interesting side note for the following decades. In the 1920's through 30's, Frumkin [26, 27] performed experiments studying the wetting behavior of an electrolyte in contact with a solid metallic electrode and exposed to a potential difference, marking the first study into what we now term electrowetting. Sondag-Huethorst and Fokkink further developed the idea and studied the effect of modifying the surface of the electrode to improve the electrowetting performance, specifically by the addition of a self-assembling monolayer (SAM) of electroactive alkanethiol to a gold electrode [28]. One of the most significant advancements came when Berge [29] introduced the use of a layer of (typically hydrophobic) electrically insulating material (dielectric) atop the electrode. This had the effect of dramatically increasing the voltage that could be applied before decomposition of the electrolyte occurred due to significant current flow. It is this last development, termed either electrowetting on dielectric (EWOD) or sometimes electrowetting on insulated electrical contacts (EIEC) which has allowed many of the previously discussed practical applications to be developed.

2.2 Governing Equations

When a voltage is applied between the electrolyte and electrode (and intervening dielectric layer) of an EWOD setup, it results in the migration of charges within the drop and underlying substrate [29]. According to Lippmann's equation, the interfacial tension σ_{SL} of the solid-liquid interface is affected by this charge migration as follows

$$\sigma_{SL} = \sigma_{SL}|_{V=0} - \frac{c}{2}V^2 \quad (1),$$

where c is the specific capacitance of the dielectric layer and V is the externally applied voltage (since for electrowetting on dielectric there exists no potential difference between electrode and electrolyte in the absence of the applied one). The contact angle between a droplet and the surface it lies upon when there is no voltage present (called either the Young's or natural contact angle) can be determined from a balance of the interfacial tensions acting on the three phase contact line. This is shown by Young's equation which predicts the natural contact angle of a droplet as a function of these interfacial tensions

$$\cos \theta_Y = \frac{\sigma_{SV} - \sigma_{SL}}{\sigma_{LV}} \quad (2),$$

where the subscripts SV and LV denote the solid-vapor (gas) and liquid-vapor interfaces respectively (see Figure 2).

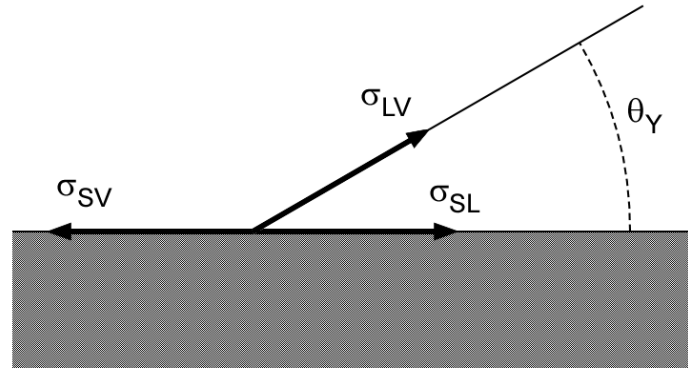


Figure 2. Schematic representation of Young's equation.

By combining the above two equations one achieves what has been called the electrowetting on dielectric or Young-Lippmann equation

$$\cos \theta = \cos \theta_Y + \frac{\epsilon \epsilon_0}{2d\sigma_{LV}} V^2 \quad (3),$$

where θ is the contact angle of the electrolyte on the dielectric, θ_Y is the contact angle at zero applied voltage, ϵ and ϵ_0 are the permittivity of the dielectric layer and a vacuum (respectively) and d is the thickness of the dielectric layer.

This equation very accurately describes EWOD behavior under most conditions [1]. In many cases, the dielectric layer will comprise 2 or more layers, oftentimes a dielectric topped with a surface treatment to provide a naturally non-wetting surface for the droplet. This added thickness has an impact on the capacitance of the system, the magnitude of which is determined by the

hydrophobic layer used (and its dielectric constant) and the thickness of layer applied. This can be accounted for by inclusion of these terms in the Young-Lippmann equation. The modified version appears below:

$$\cos \theta = \cos \theta_Y + \frac{\varepsilon_1 \varepsilon_2 \varepsilon_0}{2\sigma_{LV}(d_1 \varepsilon_2 + d_2 \varepsilon_1)} V^2 \quad (4),$$

Where the subscripts 1 & 2 denote the different layers of the composite dielectric layer (dielectric and surface treatment) [30].

2.3 Electrical Models

2.3.1 Grounded Droplet Electrical Configuration

As discussed above, electrowetting results in a reduction of contact angle in the presence of an electrical potential difference between the droplet and the electrode it lies upon. To reduce the contact angle of only a portion of the droplet (to achieve droplet motion/transport), there must exist a difference in potential only between a portion of the drop and substrate (or the potential difference between droplet and substrate must be significantly greater in one portion of the droplet compared to another). Since the droplet is a continuous mass of conductive fluid, all portions of it will be at virtually the same electrical potential. In order to achieve this asymmetry in electrical potential then, the substrate must be manipulated. In most previous work in creating droplet motion (section 1.3.2.3) the paradigm has been to use a series of small electrodes, several of

which are covered by the drop at any one time. In this way, only the portion or droplet immediately above an energized electrode has its contact angle reduced, and motion can be achieved by sequentially energizing the desired electrodes so that the leading edge of the droplet repeatedly experiences contact angle reduction, moving forward a small amount in each step.

A simplified electrical schematic of these types of devices might look something like Figure 3. The circuit consists of the droplet, a voltage source, a switch to control which of the series of electrodes is energized, and the electrode/dielectric components.

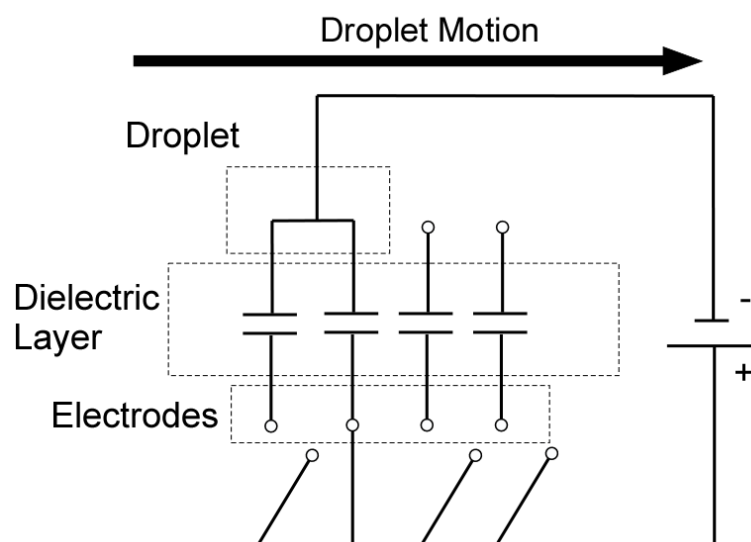


Figure 3. Idealized equivalent circuit of current EWOD designs for droplet transport.

Here the dielectric layer is modeled as idealized electrical components, namely capacitors. If a composite dielectric layer is used (a dielectric layer topped by a surface treatment) there would be a second capacitor placed in

series with the one representing the dielectric layer. In these designs, the electrode used is highly conductive and as such is modeled to be at equipotential with the applied voltage source. One may note that these designs (and many other electrowetting designs) necessitate grounding of the circuit through the top of the droplet. For cases of static electrowetting (where the droplet does not move) electrical contact can be made as simply as placing a wire into the bulk of the droplet. In cases of electrowetting where the droplet moves, a common technique has been to use a single continuous top plate electrode, so that the droplet is always grounded so long as its top remains in contact with the top plate electrode. The capacitors shown in Figure 3 represent the capacitance per unit area as used in equations (3) and (4). As shown, only one electrode is energized. As such there is contact angle reduction only on the right side of the droplet, resulting in a small motion to the right. Once the droplet has moved to cover the next electrode to the right, it will be in turn energized, and the previously energized electrode switched off. This results in another small motion to the right. In this way, an electrical potential difference is always maintained at the right hand (leading) edge of the droplet.

2.3.2 Novel Actuation Concept

The design presented in this paper achieves droplet motion in the same basic way, namely by creating a potential difference between only a portion of the droplet and substrate. However, it does so by a novel method. It was

posited that by introducing a new electrical component into the design, namely a diode, droplet transportation could be achieved using a much simpler design, that such motion would be continuous (rather than in small discrete steps) and its direction would be dependent upon the polarity of the voltage. In this new design, the entire device consists of a single circuit.

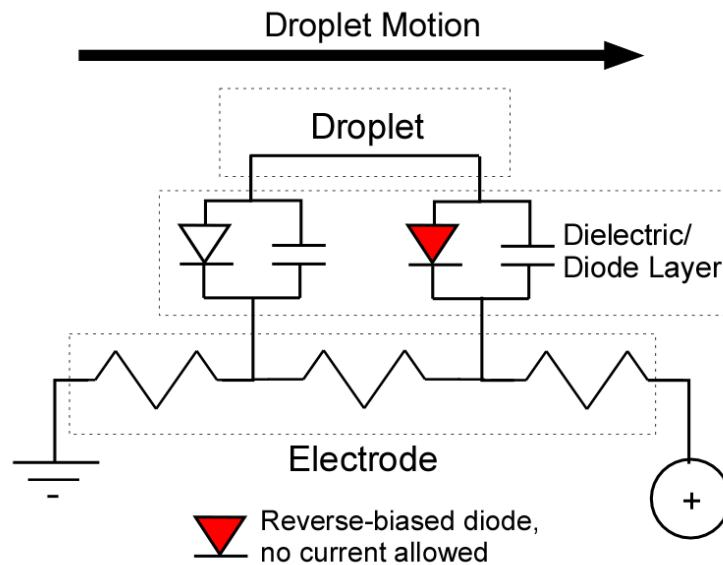


Figure 4. Idealized equivalent circuit of proposed EWOD device

If a diode and capacitor are placed in parallel, with a voltage applied across them both, the diode will either allow current flow or not, depending on the polarity. If the diode is reverse-biased, and no current allowed, charge will accumulate in the capacitor. If an array of these diode-capacitor pairs are connected at one end by resistors, and a voltage applied across this series of resistors (Figure 4) any two adjacent diode-capacitor pairs will be at a different potential (due to the voltage drop provided by the resistors). When two adjacent

sites are connected electrically on their free end by the presence of the droplet, the more positively charged site will be reverse-biased (preventing the flow of current) and the more negatively charged site will be forward-biased (allowing current flow). The result of this will be a potential difference between the droplet and electrode at the reverse-biased site but not at the more negatively charged forward-biased site. This potential difference combined with the charge accumulated in the capacitor should result in a contact angle reduction through electrowetting effects in the area surrounding the reverse-biased site, while the equipotential between the droplet and forward-biased site means the voltage in the Young-Lippmann equation is essentially zero resulting in no contact angle reduction in the area surrounding the forward-biased site.

While this result seems identical to the previous design's, where it differs is in what happens when a whole array of sites is used. To achieve further motion the previous design required the operator to switch to the next electrode in sequence to achieve another step of motion, and so on until the total motion was complete. In the new design presented here, this is not necessary. The resistance between diode-capacitor pairs provides for a voltage drop between them, resulting in each pair being at a different potential than any other. As the droplet moves to the right and covers the next-most positively charged pair, that diode will become reverse-biased, preventing current flow and resulting in a potential difference between the droplet and surrounding electrode. Meanwhile, the previously reverse-biased pair is now more negatively charged than the

newly covered pair, and as such becomes forward biased, allowing current flow and eliminating the contact angle reduction. The net effect of all this is that the droplet motion will continue automatically across the length of the electrode in the direction of positive voltage gradient until either the pattern of diodes ends or the voltage is removed, requiring no switching of individual electrodes (Figure 5). Additionally, the polarity of the applied voltage determines the direction of droplet motion, whereas most existing electrowetting setups show little to no dependence of response on voltage polarity. Another significant difference between our design and previous ones is the lack of need for a top plate electrode. On our device, the voltage is applied across the resistors (not between droplet and substrate) and the droplet only provides a parallel current path as it covers the various sites. As such, the need for a top plate electrode vanishes, allowing more leeway in designing new devices.

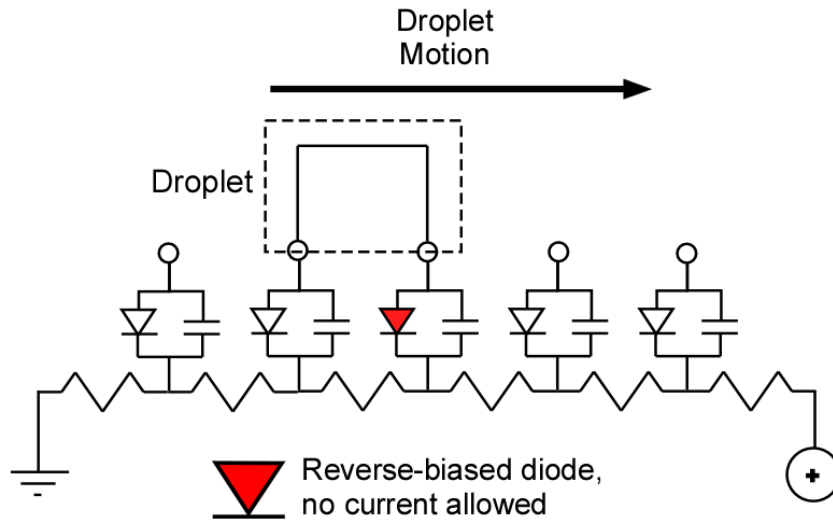


Figure 5. Array of diode-capacitor sites demonstrating how continuous motion is achieved.

2.4 Creation of Diode Sites

The main problem in constructing such a droplet transport device then comes down to translating the design in terms of idealized electrical components to one using actual physical components/features. The capacitance needed can be supplied by the addition of a dielectric layer between electrode and electrolyte, as has been done in most recent electrowetting research. The electrode can be made of a conductive substrate with a resistance appropriate to the desired voltage-current relationship. The main crux of the problem then is how to create the diodes presented in the idealized electrical schematic in section 2.3.2.

While it would be possible to construct a device using commercially available diodes of an appropriate specification, construction of such a device would be tedious and difficult at the desired size scales. Additionally a major advantage of microelectromechanical systems (MEMS) in general, and lab-on-a-chip devices in particular are their ability to be constructed using microfabrication techniques. This allows for mass production of such devices on a large scale and leads to lower fabrication costs. It would be ideal then to be able to create diode-like behavior using techniques that could be integrated into the fabrication procedures used for the remainder of the device construction. One such technique is to deposit a thin film of a valve metal onto the substrate electrode in selected areas where the dielectric layer has been removed.

2.4.1 Current Rectification in Valve Metals

As early as 1906, Gunther Schulze had demonstrated the ability of certain metals, when used as the anode in an electrolytic cell, to prevent the flow of current while allowing current to flow relatively freely when used as the cathode in the same cell [25][31]. It was noted that this behavior was present in those metals that form stable passivating oxide layers in standard atmospheric conditions. It was this current rectifying property that led to these metals being termed valve metals (ventilelektrode in the original German). In this usage, the term 'valve' is meant to relate the behavior to one-way pressure check-valves. Schulze further explored this property in several metals and using a variety of

electrolyte solutions to characterize its behavior. Metals commonly considered valve metals include tantalum, niobium, aluminum, zirconium, hafnium, tungsten, bismuth and antimony. Other elements, namely beryllium, magnesium, silicon, germanium, tin, titanium, and uranium, exhibit some of these properties and are sometimes counted in the ranks of valve metals [32].

The exact mechanism by which this current rectification behavior occurs is not settled science. The first major theory is that espoused by Schulze himself, who proposed that the valve metal anode of an electrolytic cell becomes covered with a film of oxygen over which a much thicker skin of solid oxides spreads. Since electrolytes contain no free electrons they must conduct electricity through the movement of ions, requiring much higher electrical potential gradients to pass through the gaseous film. When acting as the cathode however, it is the free electrons in the valve metal (not ions in the electrolyte) that carry the electrical charge and require much lower potentials to cross the barrier [33]. This theory contrasts with another which posits that the current rectification is a result of the porous topography typical of anodic oxide films on valve metals. Zenneck noted that with the valve metal acting as the anode in an electrolytic cell, there would be a tendency for the naturally occurring non-conductive oxide film to thicken and grow (a process known as anodization, and well understood at the time). He theorized that when the valve metal was made the anode and voltage applied, it had the effect of slightly growing the native oxide layer, reducing the access of the electrolyte to the conductive metal and preventing current flow. When the

polarity was reversed and the valve metal made the cathode, it had the effect of reducing the size of the oxide barrier and allowing current flow. In later years when the porous nature of the oxide films was realized [34, 35], it was thought that it was the reduction in the size of these pores under anodization that resulted in the reduced current flow.

A simple method of creating a structure with diode-like behavior then would be to use a small layer of valve metal between the substrate electrode and the electrolyte droplet. This would provide the current rectification necessary for the device to function as designed. Early work in using this diode-like property of aluminum films in electrowetting applications has shown the feasibility of this approach [36]. Additionally, further testing of the current-voltage relationships by the author has confirmed that the diode-like behavior of aluminum is robust and repeatable under the conditions experienced in device testing (Figure 6). For this test, a small droplet of BMIM-PF6 ionic fluid (electrolyte) was placed atop an aluminum electrode which had been treated with a thin (180 nm) hydrophobic fluoropolymer surface treatment to mimic conditions on the final device. Voltage was applied using a Kietlhey 2612A SourceMeter, with the ground contact being made with the droplet (using a platinum wire).

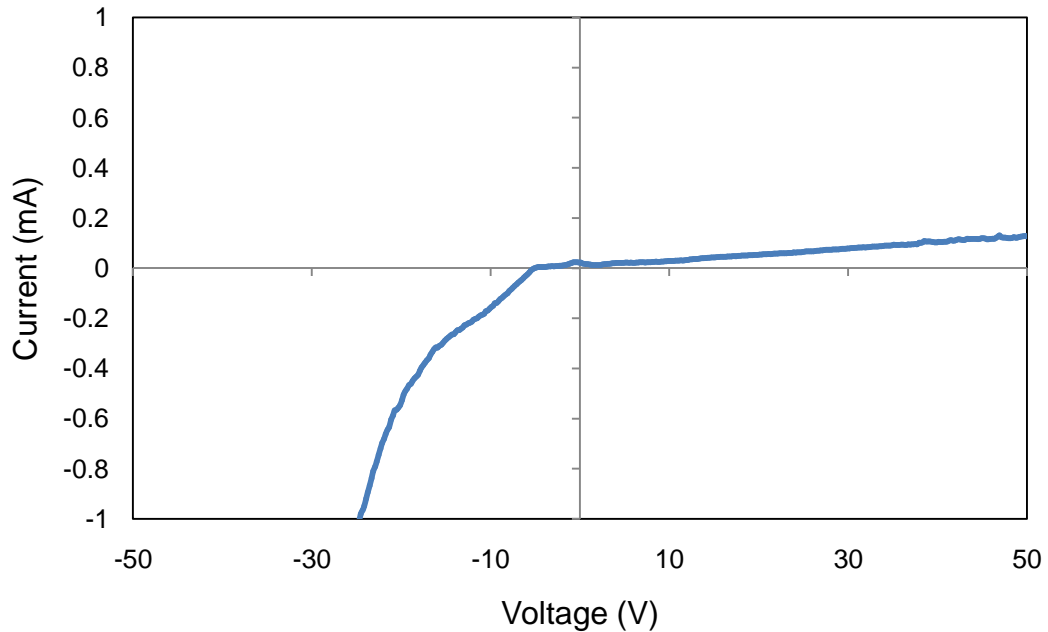


Figure 6. Current-Voltage plot of aluminum illustrating current rectifying property.

2.4.2 Alternatives for Diode Creation

In addition to the current rectification properties of valve metals in electrolytic cells, another possible technique for creation of the diodes exists. While most diodes are produced by the junction of N and P type semiconductors, it is possible to construct diodes from the junction of a metal and a semiconductor [37, 38]. This results in the creation of a Schottky barrier which has the effect of preventing current flow in one direction. These diodes are referred to as Schottky diodes and were some of the first diodes ever created (in the form of “cat’s whisker” detectors, the first semiconductor electronic device, used in early radios). If the substrate electrode onto which the valve metal layer

is deposited is made from a semiconductor material appropriate for the metal used, a Schottky barrier could be created which would aid in the one-way regulation of current through the “diode” sites.

Chapter 3.

Device Design

This chapter describes the procedure by which a design for our prototype devices was arrived at, details their specifications/dimensions, and gives the fabrication techniques used for manufacturing. The first step in our design process was to develop a predictive model of device performance, incorporating all the variables and parameters that would have significant impact on the device's functionality. This aided in designing our initial test device, and improving upon it in subsequent iterations. The model derivation is described. Following this, the actual design for our proposed device is presented, with explanations for why each component is critical to functionality, and how they each relate to the idealized electrical components discussed in the previous chapter. Lastly, the techniques used to construct the device are presented.

3.1 Device Modeling

In attempting to design a droplet transport device which takes advantage of the diode-like properties of valve metal films, it is necessary to first familiarize oneself with the various design parameters that may influence device functionality and performance. Using a device architecture as described above, even a cursory examination reveals that there are a large number of variables to

consider. With so many parameters influencing device performance, it becomes clear that a structured and organized analytical model of the device is necessary. Once such a model is developed, it may be utilized during virtually all phases of research, from the initial design phase to troubleshooting and development/improvement of the device.

3.1.1 Identification of Key Parameters

The first step in the development of such a model is to identify the parameters of device design which impact final performance. The obvious first step in this process is to explore the Young-Lippmann equation. As the fundamental model of electrowetting, the variables it uses should be adequate to characterize the electrowetting response. When examining the Young-Lippmann equation, for our purposes it is expedient to discard the two cosine terms. The only aspect of device design which will have an impact on these terms is the choice of electrolyte, ambient phase and surface treatment used (as these materials determine the natural contact angle of the droplet). These parameters (with the exception of surface treatment) are not properties of the device itself and may be easily changed in the course of experimentation. While the choice in surface treatment is an inherent property of the device itself, and not changeable once the device is fabricated, its impact on the natural contact angle can also be neglected at this point. The role the surface treatment plays as a dielectric/capacitive layer (where it will be considered) is more significant to

overall performance than its role in determining natural contact angle. In addition, most of the viable and commonly used surface treatments are variations of PTFE which have similar surface energy densities, and as such, using one versus another will have little impact on natural contact angle.

By eliminating the cosine terms from consideration, we are left with the final term. This compact term contains variables for voltage, relative static permittivities and thicknesses of the dielectric layer and surface treatment, and the surface energy density of the liquid-vapor interface (or liquid-ambient, in the case of testing done with a non-vapor as the ambient phase). It can be seen, by grouping the cosine terms in the Young-Lippmann equation to one side of the equality that this dimensionless term represents the change in contact angle after the application of the given voltage, and as such is of primary interest in characterizing electrowetting performance and will serve as a good metric to compare various designs. For the purpose of this work, this final term in the Young-Lippmann equation will be referred to as the Electrowetting Number and represented by the symbol for the greek lower-case eta. Calculation of this number will be the ultimate goal of our analytical model.

$$\eta = \frac{\epsilon\epsilon_0}{2d\sigma_{LV}} V^2 \quad (5),$$

The determination of most of the variables present in the electrowetting number is relatively straightforward. The dielectric properties of most of the more

commonly used dielectrics and surface treatments used are readily available from the manufacturer or other resources, and their thicknesses can be controlled during fabrication as well as measured afterwards by various techniques. The surface energy density of the liquid-ambient interface can often be taken from reference sources for common interfaces (air-water, etc.) and for less common electrolyte-ambient phase systems there are techniques for determining it (contact angle goniometry, or direct measurement through a tensiometer).

This leaves only the applied voltage term. For simple electrowetting setups, the voltage used in determining the electrowetting number is the entire applied voltage (as the potential difference between electrode and droplet is the total voltage applied). In the device architecture proposed here, this is not the case. With a droplet covering two valve metal sites, the more negatively charged site allows current flow while the more positively charged one is rectified and allows no current. As such, the droplet is at the same potential as the negatively charged site. Thus, the electrolyte-electrode potential difference at the leading edge of the drop (near the more positively charged site) is not the total applied voltage, but the voltage between the two valve metal sites. The voltage value used in calculating the electrowetting number, then, is not the total applied voltage, but the voltage drop along the electrode from one valve metal site to the next. Assuming the resistivity of the substrate electrode does not vary with location, the voltage drop between any two adjacent sites is merely a function of

the total applied voltage and the ratio of the site spacing (distance between adjacent sites) to total electrode length.

Another design consideration that must be made, especially with the higher voltages necessary for the proposed device architecture to function, is the current through the electrode and the power dissipated due to Joule heating. Since the manufacturers of the wafers used as substrate electrodes publish resistivity values for the various materials used in their wafers, it is necessary to calculate total resistance by using the thickness, width and length of the substrate electrode. With the resistance of a test strip and the total voltage applied across it known, the total power and energy flux (power per unit area) can be easily calculated. These numbers are useful in estimating resulting surface temperatures, and if auxiliary cooling is necessary, estimating what the capacity of such a cooling device should be.

From the preceding discussion then, a reasonable model for the electrowetting device proposed must account for the dimensional (e.g. thickness) and material (e.g. relative permittivity) properties of the various layers, the total voltage across the entire electrode, the voltage drop between adjacent sites (calculated using the dimensional parameters of hole spacing and overall electrode length), and the surface energy density of the electrolyte-ambient phase interface. If it is desirable to predict current and power characteristics of the device as well, the resistivity of the electrode as well as its dimensional properties must also be considered.

3.1.2 Define Parameter Interrelationships

Once the various parameters needed to accurately capture the electrowetting system's expected behavior have been identified, it is necessary to define the relationships between them. This was done in a spreadsheet format. This allows for all the interactions between the various separate variables to be defined, as well as for changes to one variable to be rapidly reflected in the final results. Starting with the primary purpose of the model (namely predicting the electrowetting number), the material (relative permittivity) and dimensional (thickness) properties of the possible dielectric and surface treatment layers (ϵ_1 , ϵ_2 , d_1 , d_2) are entered. Similarly, the value for the electrical constant (ϵ_0) and for the surface energy densities (σ_{LV}) of the electrolyte-ambient phase systems to be used may be entered. This leaves only the voltage left as undefined in the electrowetting number formula. As discussed above, this is not the total applied voltage, but rather the voltage drop that exists between adjacent valve metal sites. This is function of the total applied voltage (V_{tot}), the site spacing (s), and the overall electrode length (l) according to the following relationship:

$$V = \frac{s \cdot V_{tot}}{l} \quad (6)$$

While both site spacing and total electrode length are chosen at the discretion of the designer, there are limitations. The total electrode length is determined mostly by practical constraints, namely the dimension of the wafers

to be used as substrate electrodes, and the arrangement of the test strip patterns on such a wafer. Additionally, assuming site spacing is constant, a longer strip will result in a lower voltage drop from site to site for a given applied total voltage. These constraints are used as guidelines in selecting final dimensions of the design. Similarly, the choice in site spacing is at the discretion of the designer, but not completely arbitrary. Larger site spacing will result in a greater voltage drop between adjacent sites, but will also require the use of larger droplets (as a droplet must always be covering at least two valve metal sites for motion to be continuous). With a general idea of the droplet volume desired, measurements were taken to determine the typical droplet diameter for various volume droplets. Potential site spacing distances were then taken as 90% of the radius of a droplet of the given size for that spacing. With an array of various hole spacings and total electrode lengths defined, the voltage drop between adjacent sites at a given total voltage can be calculated for any combination of spacing and length. This, in conjunction with the variables defined above, allows for the calculation of the electrowetting number for any potential design

After estimation of the electrowetting performance, the second major purpose of the model is to characterize current and power characteristics of the device. With the resistivity (ρ) of the substrate material being known, the total resistance (R) of a strip of such a material is given as

$$R = \frac{\rho \cdot l}{d \cdot w} \quad (7)$$

where ' w ' is the electrode width. The width of the electrode is again a judgment call for the designer. Narrower strips are desirable in that they will increase the total resistance of the device (and hence reduce the current flow through it) and will allow for more strips to be fabricated on a single wafer. This must be balanced against the size of the droplet to be used, as the droplet must still fit on the strip. Once the total resistance of a strip has been determined, the total current through the strip at a given voltage can be easily calculated using Ohm's Law. If heat transfer considerations are a concern, it is also possible to calculate the total power consumed by the device using Joule's Law, and knowing the dimensions of the strip one can also calculate heat flux. If desired, the cooling effects from convection of the ambient phase can also be estimated using well established analytical techniques.

3.2 Device Design

As mentioned in the preceding sections, our initial test design of this novel device will be constructed using conventional microfabrication techniques, and will feature a series of layers, each contributing to the functionality of the final device.

3.2.1 Components

There are four major components to the proposed design, each corresponding to one of the idealized electrical components discussed in section 2.3.2 and presented in Figure 4. Table 1 shows a summary of the idealized components and their practical equivalent. The first component is a high-resistivity doped silicon wafer which, when built upon and diced, will serve as the substrate electrode in our design. This can be equated to the resistors shown in Figure 4. The next component, deposited atop the electrode layer, is the dielectric layer. This layer provides the majority of the capacitance needed to achieve the electrowetting effect. The most critical components are of course the valve metal sites. These are what provide the selective current rectification behavior needed for the device to function, and as such can be equated with the diodes discussed previously. The final major component consists of a thin surface treatment layer. While this surface treatment will have an effect on the total capacitance of the system (and so may be considered as a portion of the capacitor) its major impact is not as an electrical component. In addition to acting as a portion of a composite dielectric layer, it provides significant mechanical benefits to the device by providing an extremely non-wetting interface between droplet and substrate, which will be discussed in detail below.

Table 1. Equivalent electrical components

Device Component	Equivalent Electrical Component
Substrate Electrode	Resistor
Dielectric Layer	Capacitor
Valve Metal Layer	Diode
Surface Treatment	Capacitor

3.2.1.1 Electrode

When examining the principles behind this EWOD design, one can see that the voltage term used in the Young-Lippmann equation to model contact angle reduction is not the total voltage applied across the entire electrode, but only the potential difference between the two adjacent valve metal sites. This is merely a function of the total applied voltage and the spacing between sites. In order to keep this value high enough to result in a significant difference in contact angle from one side of the droplet to another (and hence cause motion) it is necessary to use voltages much higher than is typical of most recent EWOD designs where the voltage between electrode and electrolyte is the total applied voltage. To keep the current through the electrode and electrolyte at a minimum, a high resistivity substrate electrode is used. For availability and compatibility with microfabrication techniques, it was decided that a large doped silicon wafer would be used as our substrate, and once fabrication was completed individual test strips would be diced from it. Using the model presented in section 3.3, the

thicknesses and resistivities of various wafers available for purchase were inserted and the most one with the most desirable predicted performance was selected.

3.2.1.2 Dielectric Layer

As we were starting with silicon wafers as our substrate, the simplest dielectric layer to use was a thermally-grown silicon dioxide (SiO_2) layer. This provides a robust dielectric layer that is easily grown, patterned and etched with standard microfabrication techniques, and would provide satisfactory performance according to our model.

3.2.1.3 Valve Metal

In order for the necessary selective current flow to occur at regular intervals, there must be periodically spaced portions of the electrode where the dielectric layer has been removed. In the design presented here, this is achieved by patterning small circular holes (on the order of 100-200 μm diameter) in the dielectric layer. Alternative designs could include strips of removed dielectric oriented perpendicular to the direction of desired droplet motion. The effect of various patterns of holes (either a single row of holes, or a three-wide arrangement of holes) is explored during experimentation.

The spacing of the holes in the dielectric layer is a key design parameter. It must be such that for a given diameter droplet, at least two sites must always

be covered by the droplet. If at any time a droplet covered only one site, the equivalent circuit would not include parallel paths through both the substrate and electrolyte droplet (as current would only flow through the substrate) and droplet motion would cease. If on the other hand the hole spacing is made very very small, the voltage drop between any two adjacent sites would be such that the effective voltage across the drop would not be sufficient to ensure significant contact angle reduction at the leading edge.

The final piece in a functional device is the use of a valve metal layer at the bottom of the holes through the dielectric layer, separating the exposed electrode and the droplet itself. If this layer were not present, current could flow indiscriminately between electrode and droplet at all hole sites. The diode-like current rectification properties of valve metals allows for current to flow only when the valve metal is more negatively charged than the electrolyte. Since much of our previous work in exploring this diode-like behavior was done using thin aluminum films, it seemed reasonable to continue with this material. Aluminum is a valve metal which exhibits robust diode-like properties and is easy to deposit in pure layers of controlled thicknesses.

3.2.1.4 Surface Treatment

The final layer is a surface treatment applied to the entire top surface of the finished design. Previous work in EWOD has shown that the addition of a hydrophobic surface treatment aids in strong and dependable electrowetting

behavior. By increasing the natural contact angle of the three phase contact line, it allows for contact angle reductions of greater magnitude. In addition, it has been shown that a highly hydrophobic layer also reduces the severity of hysteresis. The Young-Lippmann equation indicates that the contact angle reduction for a given voltage should be identical, regardless of whether the angle is advancing or retreating (voltage is increasing or decreasing).

In reality, some difference typically exists, known as hysteresis. This hysteresis appears not to be an error in the Young-Lippmann equation, but rather a result of the non-idealized conditions experienced in real-world testing. The hydrophobic surface treatment used in this design reduces this hysteresis, allowing for more dependable performance. Also, when the intent of an EWOD design is to achieve droplet transport, hydrophobic layers tend to reduce the occurrence of 'pinning', where a portion of the droplet will stick to the substrate. This pinning can result in either the cessation of droplet motion, or if the actuation force acting on the drop is sufficient it may cause a portion of the drop to continue its motion while the remainder remains anchored to the area of where pinning occurs causing the droplet to break in two.

To reduce the chances of pinning of the droplet at the valve metal sites, the design presented here covers the entire surface of the wafer with a hydrophobic layer. On first examination it would seem that the addition of a dielectric layer atop the valve metal would reduce or eliminate the necessary current flow at the negatively charged (trailing edge) site. However the surface

treatment layer applied is very thin and has a relatively low dielectric constant. It was suspected that enough current leakage would occur across this layer that it would not significantly reduce performance [39], due to its natural porosity, and defects or other electrically conductive pathways. This suspicion was validated by successful testing of the device.

A key benefit of the hydrophobic layer is its effect on the natural contact angle of the droplet-surface interface. This helps in achieving droplet motion in two related ways. First, by starting off with a larger natural contact angle, the total possible change in contact angle is greater. Secondly, since the actuation force acting on the droplet is the result of the asymmetry in contact angle from leading to trailing edge, the greatest actuation force is achieved by having the greatest possible natural contact angle and reducing it to the lowest value possible on the leading edge.

As mentioned above, the additional thickness provided by the hydrophobic layer and its dielectric properties has the effect of increasing the total capacitance between electrode and droplet, which has an impact on the predicted electrowetting performance. The magnitude of this impact is determined by the hydrophobic layer used (and its dielectric constant) and the thickness of the applied layer.

In previous work in electrowetting and exploration of other surface energy effects [36, 40, 41], we had familiarized ourselves with CYTOP™ 809M (Asahi

Glass) as a useful surface treatment. This fluoropolymer provides a large natural contact angle, and is easily laid down in thin consistent-thickness coats.

3.2.2 Fabrication Techniques

As mentioned previously, the design presented here was manufactured using standard microfabrication techniques, including thermal oxidation, photolithographic patterning and etching, electron-beam vapor deposition, and spin-coating. During the following discussion it may be helpful to refer to Figure 7.

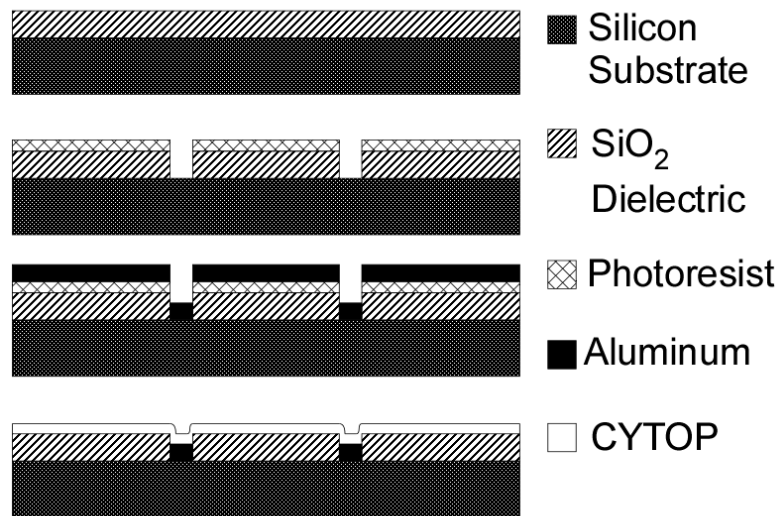


Figure 7. Construction techniques for electrowetting device. *Top*: Si substrate with SiO₂ dielectric layer. *Top Middle*: Photoresist layer after patterning and etching. *Bottom Middle*: Aluminum layer applied by electron beam deposition. *Bottom*: Photoresist is removed in liftoff procedure along with unwanted aluminum, leaving aluminum layer in previously patterned holes in dielectric layer. Entire top surface is given CYTOP surface treatment

The substrate used for all iterations so-far produced was a 4" diameter 270 μm thick wafer of [111] silicon N-doped to a resistivity 300-500 $\Omega\text{-cm}$. Using our predictive model (and assuming test strip widths of 8.98 mm) this would result in Joule heating of 0.37 to 0.62 W/cm^2 depending on where in the range of given resistivities the wafer is. Atop this wafer an oxide layer was grown using dry thermal oxidation to a final oxide thickness of 480 nm (as determined by profilometry measurements).

After oxidation of our initial wafer, several more wafers were oxidized simultaneously in a separate batch to the same final thickness, with those not ready for immediate further processing set aside for later use. Later in the testing process, it was decided that it would be desirable to fabricate wafers with a slightly thinner oxide layer. Before further processing of these wafers, they were immersed in a standard hydrofluoric acid buffered oxide etch (BOE) to reduce total thickness to approximately 400 nm. Once the wafers held the desired thickness of oxide, they were prepared for photolithography.

This begins by first spin-coating a primer of Hexamethyldisilazane (HMDS) to ensure a good bond between oxide and photoresist. After priming, a layer of Shipley S1813 positive photoresist was applied via spin-coat. After spin-coating the wafer was subjected to a soft bake on a hotplate at 100°C. It was then masked and exposed, then submerged in Microposit MF-319 developer to remove the portions of photoresist that were exposed to UV during the exposure

step. After a hard bake for one minute at 100°C the now-exposed portions of oxide were etched away down to bare silicon by BOE.

After the photolithographic process is completed, but before removal of the unexposed photoresist, the entire wafer was coated with a layer of aluminum using electron-beam physical vapor deposition. Final thickness of the aluminum layer was 300 nm as determined by previous calibration/characterization of the deposition process. This step results in aluminum covering the entire wafer, while the desired result is to have aluminum only at the bottom of the holes etched in the dielectric layer during photolithography (as well as small strips of aluminum deposited directly to the substrate electrode on each end, to aid in making electrical contacts). Since the photoresist layer remains (from previous steps) covering all those areas which still have an oxide layer, when it is removed by rinsing in acetone it takes with it the aluminum that was deposited atop it. After this liftoff procedure, the result is a silicon wafer with an oxide layer atop it. In this oxide layer are a series of patterned holes, at the bottom of which (deposited directly atop the bare silicon) each contains a layer of aluminum.

All that remains is the surface treatment layer. The initial test wafer design called for a final CYTOP thickness of 180 nm. This was achieved using a spin-coat program as detailed in Table 2. For each step, once the final spin speed is reached it is maintained until the total step duration has been reached.

Table 2. Standard-thickness CYTOP spin-coat program

Step	Initial Speed (RPM)	Accel. Rate (RPM/s)	Final Speed (RPM)	Total Step Duration (s)
1 Acceleration	0	336	500	10
2 Acceleration/Constant	500	840	1800	20
3 Deceleration	1800	-672	0	-
4 Curing	Soft bake in oven, 100°C for 30 minutes Hard bake in oven, 200°C for 60 minutes (immediately following soft bake)			

As testing progressed, it was decided to test wafers with a thinner surface treatment layer. It was thought that the reduced thickness would increase the specific capacitance of the device and decrease the voltage necessary for actuation. For these wafers a different spin-coat program was used, which can be seen in Table 3.

Table 3. Reduced-thickness CYTOP spin-coat program

Step	Initial Speed (RPM)	Accel. Rate (RPM/s)	Final Speed (RPM)	Total Step Duration (s)
1 Acceleration	0	336	700	10
2 Acceleration/Constant	700	840	4500	40
3 Deceleration	4500	-672	0	-
4 Curing	Soft bake in oven, 100°C for 90 seconds Hard bake in oven, 180°C for 60 minutes (immediately following soft bake)			

Once the surface treatment has been applied, the final step before testing can commence is to dice the wafer into its individual test strips. The overall wafer design is presented below in Figure 8.

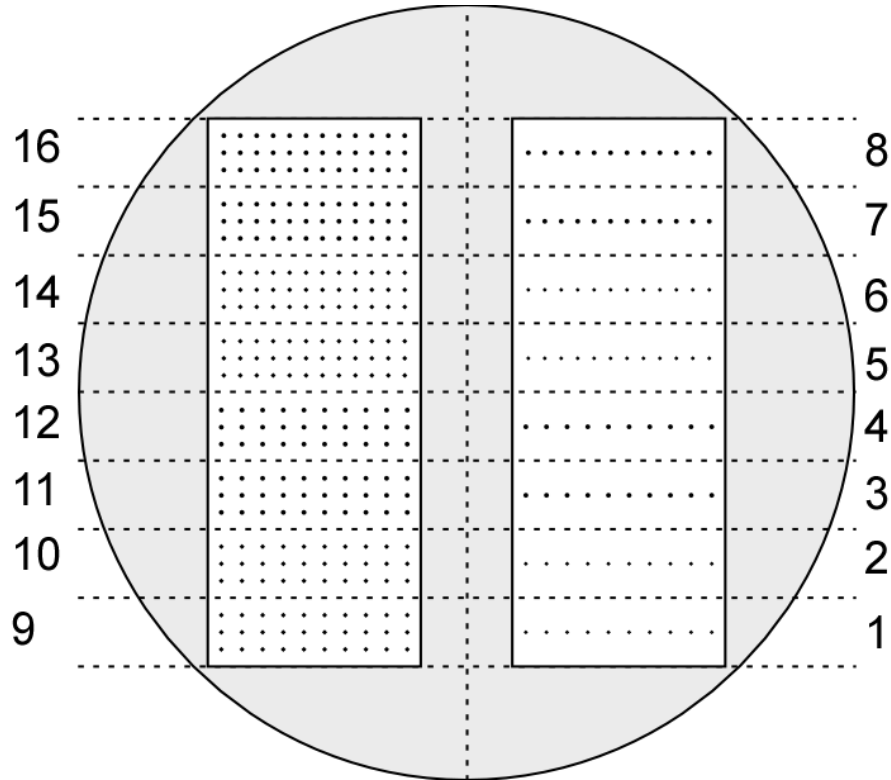


Figure 8. Wafer pattern schematic. Grey areas and small circles are where oxide etching occurs (and where aluminum remains after liftoff). Dotted lines indicate where dicing is to occur, resulting in 16 final test strips.

The following tables list the various dimensions and properties of the strip/site patterns (which are identical for all wafers produced) (Table 5) and for thickness of the different layers (different from wafer to wafer) (Table 4)

Table 4. Wafer layer dimensions

Wafer	Oxide Thickness (nm)		CYTOP Thickness (nm)		Aluminum Thickness (nm)
	Profilometry	Ellipsometry	Profilometry	Ellipsometry	
1	480	-	180	-	300
2	-	440-460	-	40-60	300
3	-	530	-	180	300
4	-	522	-	40-50	300

Table 5. Strip/Site dimensions

Strip #	Site Diameter (μm)	Site Spacing (mm)	Site Pattern
1	100	2.71	Single Row
2			
3			
4	300	2.16	
5			
6			
7			
8	200	2.71	
9			
10			
11	300	2.16	Triple Row
12			
13			
14	200	2.16	
15			
16			

Refer to Figure 9 for a diagram of a generic test strip (not to scale). For all strips, the test area (the rectangle of remaining oxide layer) measures 27.9 mm x 8.9 mm. Two different site spacings were used, calibrated for droplet volumes of

30 μl and 50 μl (to ensure that a droplet would always cover a minimum of 2 sites). For all strips, the sites are centered both laterally and longitudinally within the test area. For those strips featuring a three-wide site pattern, the rows of sites are laterally separated by 2.25 mm.

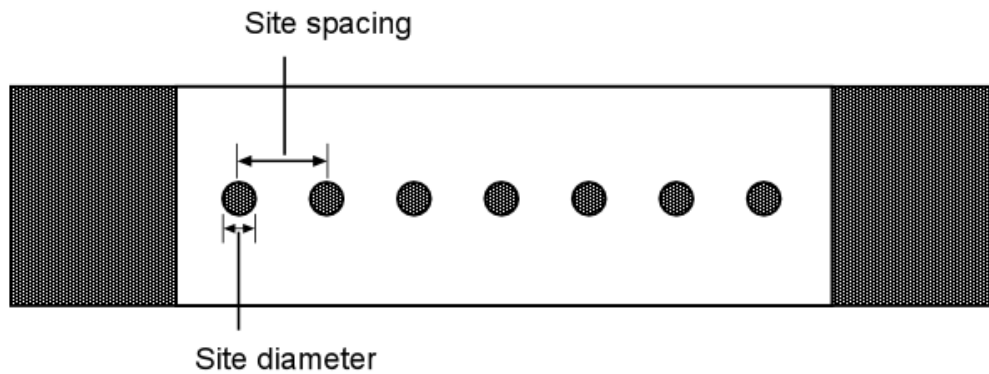


Figure 9. Generic test strip diagram.

Chapter 4.

Device Testing

For evaluation and testing of the various strips, a relatively simple procedure was established. The strip would be placed in a small dish and if an ambient phase other than air is being tested, the dish is filled with an appropriate volume of the selected ambient phase. A droplet of the electrolyte being tested is dispensed onto the strip near one end. When the setup is complete, voltage is applied across the test strip. Each test run lasts 20 seconds, during which the total applied voltage and current through the strip are recorded. Additionally, during each test run digital images are captured from a remotely triggered camera mounted in a top-view configuration. The square-wave trigger signal used for the camera is also recorded so that each image can be exactly correlated with data points from the voltage and current plots.

4.1 Experimental Variables

During testing, there are several experimental variables that are under the control of the tester. The most obvious one is the strip being tested, which determines the site spacing, diameter and pattern (based on strip number) as well as the thicknesses of the various layers present (based on wafer number).

Additionally, the tester may select the electrolyte being used and the ambient phase --both of which have significant impact on final device performance.

Electrolytes used in testing include deionized water, 1-Butyl-3-methylimidazolium hexafluorophosphate (BMIM-PF6, an ionic phase fluid, Acros Organics) and 1 M sodium sulfate (Na_2SO_4) solution. Ambient phases tested under include air and n-Hexadecane 99% (Alfa Aesar). The final variable at the tester's discretion is the voltage being applied. It was decided early in testing that the two major metrics of device performance we would be examining were the minimum voltage required for steady consistent droplet motion, and droplet velocity at a given voltage. In order to test for these, two different voltage profiles were used. For minimum actuation voltage testing, the voltage was manually ramped up from a pre-selected low bound throughout the test run. If no motion was detected testing was repeated with a higher initial voltage. An examination of the digital images captured reveal when droplet motion began, and can be used to correlate that to the voltage being applied at the time. Once a range of typical minimum actuation voltages was determined, a set voltage was chosen at which to perform velocity measurements. For these tests, the voltage was switched on and remained constant through the entire test.

4.2 Testing Setup

4.2.1 Equipment

The basic testing setup consists of a Matsusada Precision Inc. RG-360-0.2 power supply, a National Instruments Inc.(NI) cDAQ-9172 compact DAQ chassis connected to a desktop PC, a NI 9219 4-channel analog Input Module, and a testing circuit. The testing circuit consists of a standard breadboard and resistors wired so as to allow determination by the DAQ of total applied voltage across and current through the wafer. One portion of the test circuit is a low-resistance ($10\ \Omega$) resistor wired in series with the test strip which, by measuring the voltage drop across it and its known resistance, can be used to determine current through the wafer by Ohm's Law. Typical currents through the wafer were approximately 10 mA (at 370 volts, the maximum tested). The second portion of the testing circuit consists of a two-resistor ($10\ \text{k}\Omega$ and $1\ \text{M}\Omega$) voltage divider wired in parallel with the wafer/current-measurement circuit. The magnitude of the resistors was chosen to be sufficiently high that significant amounts of current would not flow through this parallel path but rather through the strip (the total strip resistance being approximately $0.05\ \text{M}\Omega$ compared to $1.01\ \text{M}\Omega$ for the voltage divider). The voltage drop measured across the lower-resistance resistor will be within the measurement range of the 9219 DAQ module ($\pm 60\ \text{V}$), and the total applied voltage (potentials up to 370 V were used) can be determined from the ratio of the two resistors in parallel with the test strip.

If it was desirable to measure the total current through the entire testing circuit (rather than just through the strip) the $10\ \Omega$ resistor could be moved to before where the two parallel circuits (the strip and voltage divider) split, immediately downstream of the negative terminal on the power supply.

In addition to the main testing setup, it was also necessary to capture images at specific time intervals to correlate droplet motion with the current and voltage data at a particular time. The camera used was an Edmund Optics EO3112C, manufactured by IDS Imaging, which features built-in hardware trigger capability, allowing it to be remotely triggered via a square-wave voltage signal. To control this functionality a 5 Hz square-wave signal is generated in the PC and output through an NI 9263 4-channel Output Module. This module is not capable of providing enough power to dependably trigger the camera, so this square wave signal is used to operate an E13005 NPN power transistor which switches power to the camera from a separate Elenco Precision XP-581 power supply. Figure 10 shows a schematic representation of the testing setup.

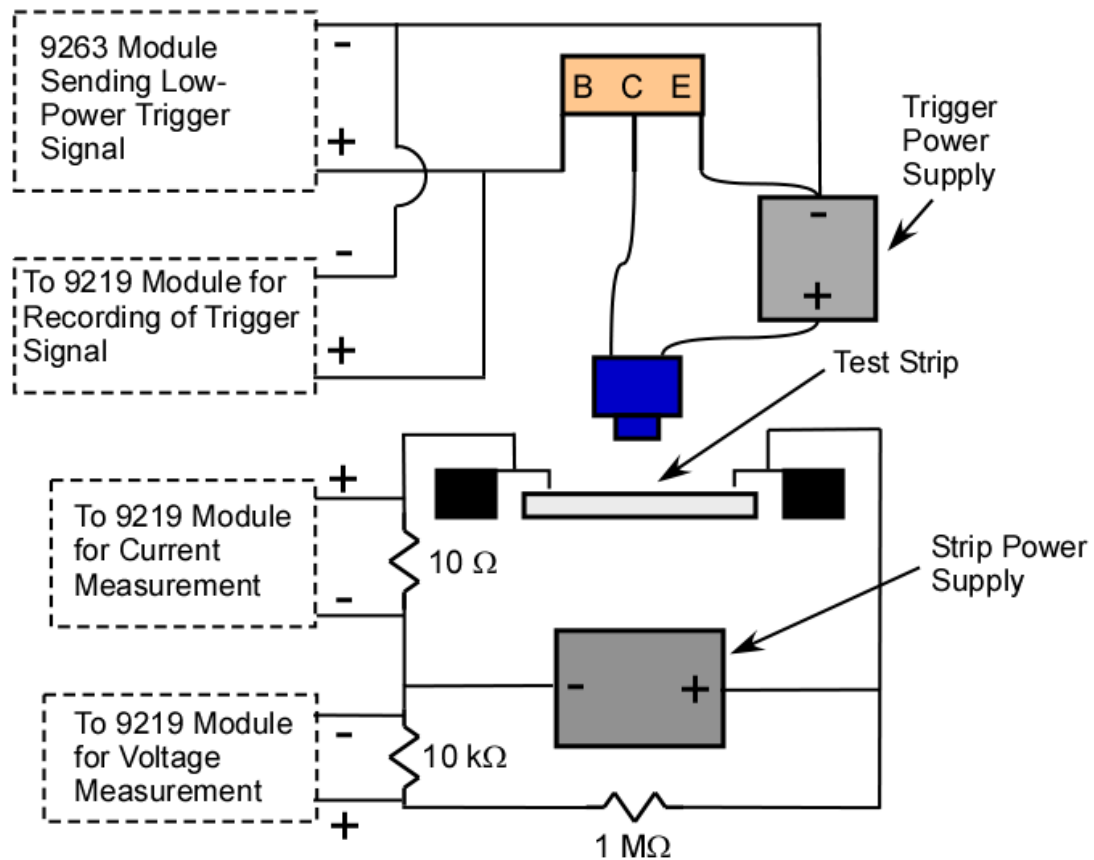


Figure 10. Testing equipment schematic.

While the camera manufacturer provides development code to interface with their camera, some modification was needed to achieve the desired functionality. A code segment which receives the trigger signal and uses it to save the image from the camera to memory is provided, but was modified to also write the triggered image file to the hard disk at each trigger signal. See Appendix A for the modified portion of the development code.

4.2.2 Testing Procedure

As discussed above, the setup for testing is simple. With the testing equipment in place and connected, the strip being tested is placed into a reservoir. If an ambient phase other than air is being used, the reservoir is filled with the desired phase to a level that would prevent the electrolyte droplet from interacting with the air-ambient interface. While ambient phase depth was controlled in as much as interference with the electrolyte droplet was eliminated, the exact depth was not kept accurately consistent. With the relatively large size of droplets used (compared to many other microfluidic devices) the effect of pressure due to the mass of ambient fluid may play a more significant role (relative to surface tensions effects) in droplet behavior. In further testing it would be advisable to use a measured and consistent ambient phase depth to eliminate this source of potential variability in results. Electrical contacts with the test strip are made via tungsten probe tips (held in micropositioners) contacting the aluminum pads left for this purpose on the end of each strip. With the strip secured and covered by ambient phase material, the desired volume of electrolyte is dispensed onto one end of the strip, with care taken to ensure it is centered laterally. The PC software used to interface with the DAQ as well as the customized software for camera operation are initialized. Lastly the operator ensures that the testing circuitry is connected properly and that the Elenco 'trigger' power supply is powered up and the Matsusada 'strip' power supply is on in standby mode.

The operator begins by initiating a test run in the data acquisition software, which we selected to last 20 seconds. Once data is recording, the operator switches the strip power supply on from standby and sends the wafer the desired voltage profile (either constant voltage for velocity measurement or manually ramped for minimum actuation measurements). When the test run is concluded the strip power supply is returned to standby. After a test run any necessary adjustments can be made (dispensing another electrolyte drop, changing strip, changing voltage polarity, etc.) and further testing can continue.

After the conclusion of a testing session, the software programs can be closed, and the power supplies turned off. The testing reservoir is emptied and cleaned in a manner appropriate to the ambient phase being used. The used test strips are carefully cleaned to prevent deterioration and ensure consistency between testing runs. The strips were rinsed first in acetone, then methanol, and finally deionized water, and dried under a stream of compressed air.

4.3 Results

The initial goal of early testing was to determine if the proposed system would indeed be capable of producing continuous droplet motion. As such, a wide variety of strips (1, 3, 5, 7, 9, 11, 13, and 15 from Wafer #1) were tested first using deionized water as the electrolyte under an air ambient phase. Under these conditions the maximum voltage from the strip power supply was needed to achieve any reaction from the droplet, and this reaction was usually limited to a

slight elongation of the droplet, with very small motion occasionally being observed. It seemed clear that the expected force was acting on the droplet, just not with a magnitude sufficient to cause motion. This result is not entirely unexpected as DI water makes a poor electrolyte, due to its lack of significant charge carriers, and shows poor current rectification properties when used atop aluminum.

Testing was expanded to include the use of hexadecane as the ambient phase which increased the mobility of the droplets slightly, but still was insufficient to attain dependable consistent motion. Hexadecane was chosen due to the lower surface tension of a water-hexadecane interface compared to a water-air interface (45 vs. 71 mN/m as measured by a Du Noüy ring tensiometer) while remaining non-conductive, and immiscible with water or aqueous solutions. This lower surface tension value should increase the electrowetting number (and device performance) for a given voltage. Additionally the use of oil ambient phases has been shown to yield higher consistency of results with less contact angle hysteresis. The next testing phase included testing of other electrolyte fluids. Success was achieved using the ionic fluid BMIM-PF6 as the electrolyte, under an ambient phase of hexadecane. Figure 11 shows a photocompilation demonstrating droplet motion during an early successful test run. While with this setup droplet motion was consistently achieved, the voltages necessary for most strips were at or near the limits of our power supply (nominally rated to 360 V, in reality capable of closer to 380 V). An ionic fluid was chosen due to previous

work demonstrating the electrowetting performance of this class of electrolyte [42-44]. It is suspected that the larger size of the charge-carrying particles (ions) in these fluids helps reduce the occurrence of current leakage through small defects in the dielectric layer.

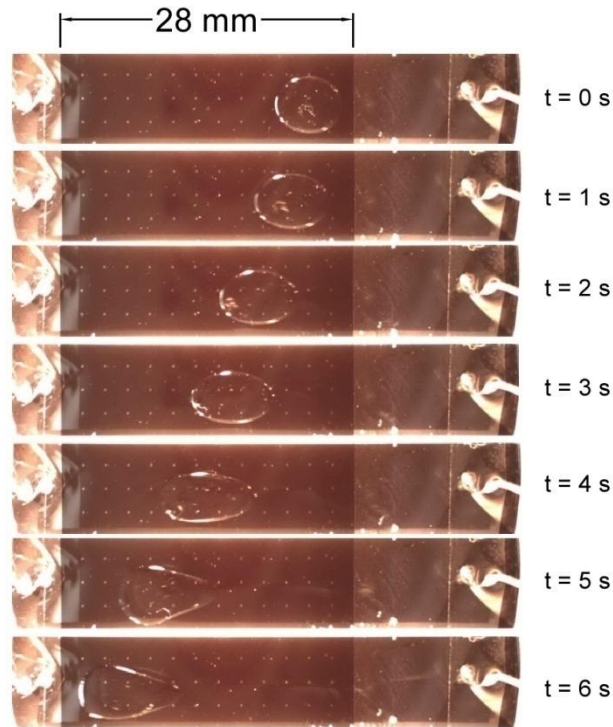


Figure 11. Photocompilation of successful test run. The strip shown is number 13 (see Figure 8) from Wafer 1, with BMIM-PF6 as electrolyte and hexadecane as the ambient phase.

In an attempt to reduce the operating voltages to a lower range, further wafers were fabricated with reduced surface treatment thickness (Wafer 4), and with reduced surface treatment and dielectric layer thicknesses (Wafer 2). The reduced thickness should have the effect of increasing the specific capacitance

of the interface and therefore reducing the voltage necessary to cause the same contact angle reduction. Additionally, another wafer (Wafer 3) was constructed with the same specifications as the original test wafer (Wafer 1). Unfortunately neither Wafers 2 or 3 showed significant success in testing.

With Wafer 2 it was thought that the reduced thickness of both the surface treatment and dielectric layers was to blame, reducing the effectiveness of the dielectric or allowing defects present in the material to provide conductive paths through to the substrate electrode. Current-voltage relationship testing on strips from Wafer 2 supports this, as it showed significant current flow through some portions of the dielectric layer with this reduced thickness as can be seen in Figure 12. Current-voltage testing on test strips was performed in the same manner as described in section 2.4.1 for Figure 6.

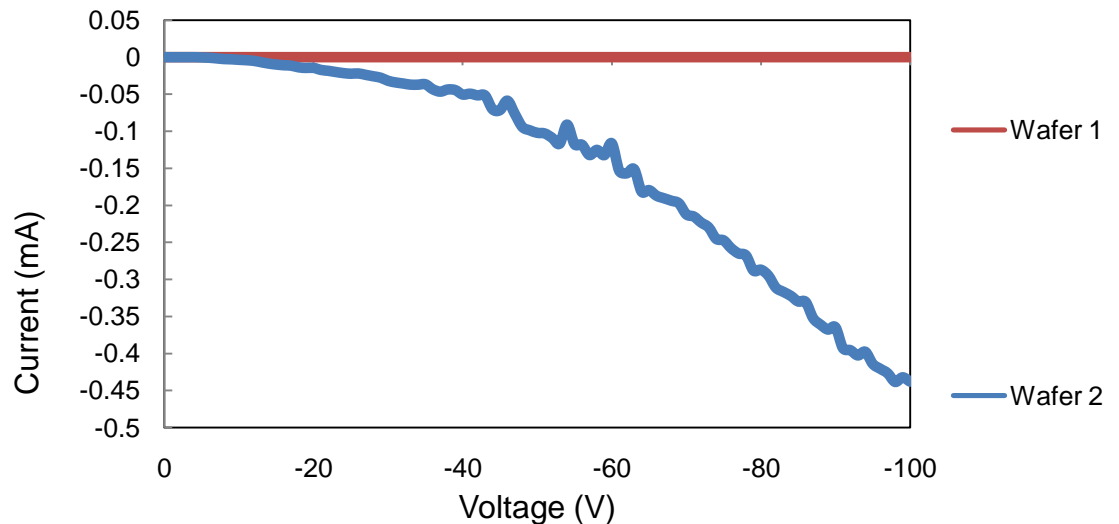


Figure 12. Current-Voltage plot for Wafer 1 and Wafer 2 dielectric layer. Testing was performed with droplet covering only dielectric, no aluminum sites. These results indicate failure of the thinner dielectric layer in Wafer 2.

Wafer 3 was an almost complete failure, with no significant successful tests on any of its strips. This seems anomalous, as it has dielectric layer and surface treatment thicknesses identical to Wafer 1 (which showed moderate success). Later measurement through ellipsometry confirms these thicknesses. It was suspected that an unknown error in the fabrication process resulted in some defect which prevents proper functioning. It seemed likely the problem lies with the aluminum deposition as the oxide layers for wafers 2-4 were grown simultaneously and the surface treatment is the proper thickness. This supposition was confirmed when testing revealed that no current would flow through any sites, regardless of the polarity applied as demonstrated by Figure 13. Contrast this with the expected diode-like response seen in Figure 6.

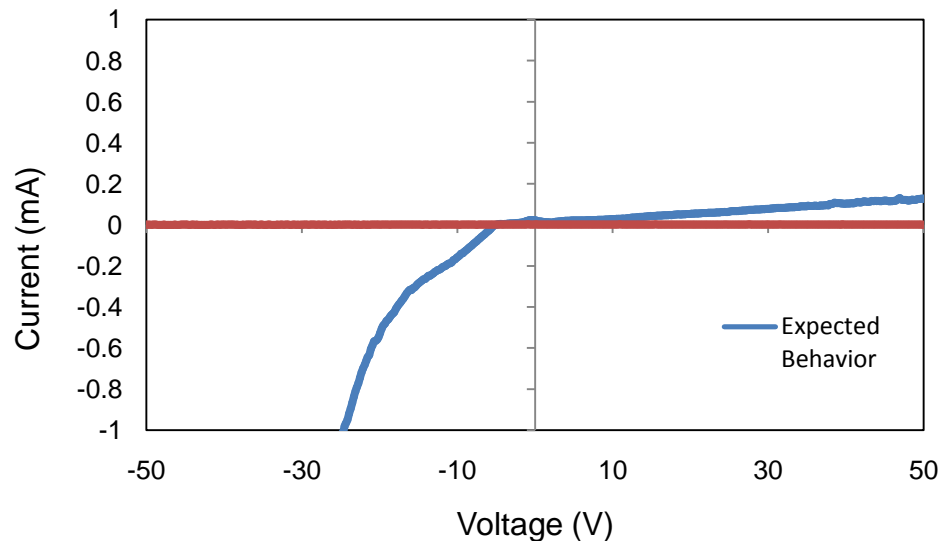


Figure 13. Current-Voltage plot of aluminum site on Wafer 3. This plot shows the lack of any significant current flow between electrode and droplet through the aluminum site. Compare to the expected behavior, reproduced here from Figure 6.

Wafer 4, however, worked consistently and the required voltage was within the capability of our power supply. From this point on, all of the testing to assess velocity and minimum actuation voltages were carried out on Wafer 4. This was done to reduce the number of variables influencing device performance. After testing was performed on all strips using BMIM-PF6 as the electrolyte, another attempt was made to reduce voltage requirements even further.

A fellow researcher exploring the diode-like properties of aluminum under electrolytes had tested several different electrolyte solutions to determine which, if any, showed the strongest diode-like behavior. At his suggestion, a 1 molar solution of Sodium Sulfate (Na_2SO_4) was used in testing, and showed significant improvements in voltage required and droplet velocity. While some of this is certainly due to the lower surface tension and viscosity of the fluid, the stronger current-rectifying properties of aluminum when under Na_2SO_4 are also likely significant contributors.

4.3.1 Minimum Actuation Voltage

Once initial testing to determine which combination of electrolyte and ambient phase, as well as which wafer configuration (SiO_2 and CYTOP thicknesses) was most effective, testing was begun to characterize the performance of the different strip design present on each wafer. All of the comparative testing was performed on Wafer 4, which showed the most

promising results in initial testing. This was done to enable direct strip-to-strip comparisons of results, with no influence from wafer configuration. Additionally, all testing was completed using BMIM-PF6 as the electrolyte and hexadecane as the ambient phase. The first performance metric tested for was minimum actuation voltage. This was determined by performing several test runs on each strip in each direction, with the voltage ramping up from a lower initial value (usually around 150 V) until droplet motion was detected. Upon completion of test runs, the photos taken during testing are examined to determine at what point smooth continuous droplet motion began. By correlating the sequence number of the frame in question to the recorded trigger signal, the time at which that picture was taken can be determined, and the voltage at that time noted.

In many instances, the droplet motion did not have a clear-cut 'turn on' point, but rather would begin by distending and elongating in the direction of voltage gradient. Additionally, it was common for the droplets to move forward a small tiny step at a lower voltage and remain stationary until a higher voltage was reached. It is estimated that this was the result of defects or imperfections on the strip surface resulting in the anchoring or pinning of a portion of the drop to the substrate. As such, there were significant variations in the minimum actuation voltages recorded on a given strip, as can be seen in the standard deviations given. In Table 6 the average of all minimum actuation voltages recorded for a given strip are listed, along with their standard deviations. In all results tables, the strip number is given according to the convention Wafer_Number.Strip_Number

where 'wafer number' corresponds to those given in Table 4 and 'strip number' to those listed in Figure 8.

Table 6. Results for minimum actuation voltage on Wafer 4

Strip #	Site Diameter (μm)	Site Spacing (mm)	Site Pattern	Average Minimum Actuation Voltage (V)	Standard Deviation (V)
4.01	100	2.71	Single Row	303	-
4.02				364	16.3
4.03	300			332	44.5
4.04				342	47.3
4.05	100	2.16		352	33.2
4.06				323	42.9
4.07	300			367	12.1
4.08				341	48.1
4.09	200	2.71	Triple Row	326	53.7
4.10				349	24.7
4.11	300			346	12.0
4.12				363	3.5
4.13	200	2.16		366	0.7
4.14				370	22.6
4.15	300			364	24.0
4.16				371	16.3

4.3.2 Droplet Velocity

Droplet velocities were determined in a method similar to that used in determining actuation voltages above. Test runs were conducted, this time using a constant voltage profile. Since the minimum actuation voltages for many strips were at or near the maximum output of the strip power supply, a constant voltage

of 370 V was chosen for all velocity testing done. Even with this, there were several strips which would fail to actuate at this voltage, or do so inconsistently such that only one good test run was acquired. These can be noted by the hash marks placed in either the velocity or standard deviation columns in Table 7 below, which shows the results of velocity testing. Again, velocities listed are averages of all runs completed on a given strip.

Table 7. Results for droplet velocity on Wafer 4.

Strip #	Site Diameter (μm)	Site Spacing (mm)	Site Pattern	Average Droplet Velocity at 370 V (mm/s)	Standard Deviation (mm/s)
4.01	100	2.71	Single Row	2.72	0.41
4.02				6.46	2.37
4.03	300			4.01	0.71
4.04				4.43	0.44
4.05	100	2.16		5.59	3.55
4.06				4.11	-
4.07	300			3.43	-
4.08				3.26	0.16
4.09	200	2.71	Triple Row	2.32	0.55
4.10				2.83	0.18
4.11	300			3.02	0.20
4.12				2.10	0.23
4.13	200	2.16		0.8	-
4.14				-	-
4.15	300			0.77	-
4.16				0.82	-

4.3.3 Further Testing

As mentioned above, after most of the testing presented here was completed, an attempt was made at further increasing device performance by using a sodium sulfate solution as the electrolyte. This had the effect of dramatically improving device performance. Not only did minimum actuation voltages drop and velocities increase, but the dependability of the response was dramatically better. During minimum voltage testing, the droplet was much more likely to have a clear-cut start to its motion, without nearly as much of the elongation or start-stop behavior of other tested electrolytes. While the defects that are suspected to have caused these problems likely still existed on the test strips, it seems the increased actuation force, lower viscosity and lower surface tension of this fluid (over BMIM-PF6) were such that they did pose as significant an obstacle to droplet motion.

Table 8. Testing results for 1M Na₂SO₄ under hexadecane

Strip Number	Average Minimum Actuation Voltage (V)	Standard Deviation (V)	Average Droplet Velocity at 300V (mm/s)	Standard Deviation (mm/s)
4.12	198	13.5	10.11	1.71

As can be seen in Table 8 the results for testing with sodium sulfate are significantly better. On one of the minimum actuation voltage tests, very clear and steady droplet motion was seen at as low as 185 V, and the best results for

an individual velocity test was 13.82 mm/s. It seems then that further work should focus on using this electrolyte solution due to its dramatically increased performance and noticeably better consistency. The numbers presented for velocity are especially more significant when one notes that velocity tests for this electrolyte were performed at much lower voltage than in the previously given data.

4.3.4 Analysis

In analyzing the testing results, some immediate conclusions can be drawn. The biggest gains found in device performance were through careful selection of electrolyte and ambient phases. By switching first to ionic fluid, then a sodium sulfate solution, huge reductions in required voltage and increases in velocity were seen. However, this must be kept in the proper perspective. The reduced voltage requirements and increased consistency of results that arises from using more desirable electrolytes will likely be very useful in further research into this area. It should enable further testing to reveal more subtle trends in performance that depend on site parameters (diameter, spacing and pattern) that may be lost in the variability or 'noise' of the current data. However, the practical benefit (outside of research) of using specific electrolytes to reduce operating voltages is much less. In many of the intended lab-on-a-chip applications of this technology, the electrolyte used will be dictated by the purpose of the device. Bio testing devices must be able to transport a variety of biological fluids and some

designs may need to also move droplets of reagents or various other chemicals as part of the testing being performed. In these cases, achieving a lower voltage requirement by tailoring the electrolyte may not be possible.

It is less clear what the impact of thinner dielectric and surface treatment layers is. According to the Young-Lippmann equation, a reduction of the thickness should provide an increase in performance, but this must be tempered by the possibility of reducing the thickness to the point that conduction across it occurs, as appears to have happened with Wafer 2. The one successful wafer to come out of the second batch, Wafer 4, features only a reduced thickness on the surface treatment layer. While this reduction in thickness must needs increase the specific capacitance of the system, both our predictive model and testing show that the difference arising from an approximately 100nm reduction would be small, if not negligible.

When analyzing the minimum voltage and velocity data for strips from Wafer 4, no dramatic and clear-cut trends (with respect to site spacing, size or pattern) emerge on first examination. The minimum voltages recorded vary between test runs on a single strip by as much or more as they do between different strips, making it difficult to draw any conclusions from this testing. While there may be some dependence of minimum actuation voltage of the site diameter and site pattern, it is less than the magnitude of the variability of the data recorded. With regards to site spacing, it seems very likely that this would have an impact on minimum actuation voltage, as for a given applied voltage, the

voltage drop between any two adjacent sites will be lower for a smaller site spacing distance. Since it is this voltage drop which exists between the droplet and electrode at the leading edge, reducing this value should reduce the magnitude of the electrowetting response. Some evidence of this can be seen in the voltage data. If one compares the average voltage for strips 4.01-4.04 (335V) to the average of strips 4.05-4.08 (346V), and similarly that of strips 4.09-4.12 (345.8V) to strips 4.13-4.16 (367.8V) so that the only difference between compared groups is the site spacing, there does appear to be a trend of increasing voltage requirements with decreased site spacing. With the large variability of the data though, it is difficult to draw any definite conclusions.

To shed further light on the impact of the various strip parameters, a 3-way analysis of variance (ANOVA) was performed on the minimum actuation voltage data, with the site diameter, site spacing and site pattern serving as the three factors. As was expected, the ANOVA did not indicate that the null hypothesis could be rejected with regards to any of the three factors. In ANOVA an arbitrary cut-off point is picked for probabilities (often 0.05 or 0.01) below which it is considered safe to reject the null hypothesis. As can be seen from Table 9 below, none of the p -values found for any of the three factors was low enough to establish statistical significance, though site spacing is significantly closer than the others. More extensive testing, possibly with a more consistent electrolyte-ambient phase system, may reveal significance not shown in this data.

Table 9. *P*-values from ANOVA performed on minimum actuation voltage data

Site Diameter	Site Spacing	Site Pattern
0.7837	0.2282	0.4988

The velocity data presented is somewhat more insightful. The major trend noticed is a significantly lower velocity for those strips featuring a three-wide site pattern. Direct comparison can be made between strips 4.15/16 and 4.07/08 as these groups share identical site diameters and site spacing (300 μm and 2.16 mm respectively). Similarly strips 4.11/12 and 4.03/04 differ only by their site pattern. By looking at this data it seems the single-row site pattern shows significantly higher velocities. It is suspected this is due to the force acting more longitudinally when in the single-row configuration. The electrowetting force acting on the three-phase contact line will be normal to the contact line. In a single-row setup, assuming the droplet is centered on the strip, the force will act fully along the direction of desired motion. In a three-wide configuration, the two outer sites have the effect of pulling the droplet at an angle from the desired direction of travel. While these opposing forces would tend to cancel each other out (allowing the droplet to remain centered) it is suspected it would result in reduced efficiency of motion, resulting in lower velocities. Alternately, this could be due to increased frictional interaction with the substrate. It was noted that when using a three-wide configuration that the droplet would assume a

dramatically tear-dropped shape (Figure 14), with the leading edge spreading to cover a significantly wider portion of the strip than during single-row testing. This increase of contact area between droplet and substrate would increase the impact of friction on the droplet, reducing its velocity.

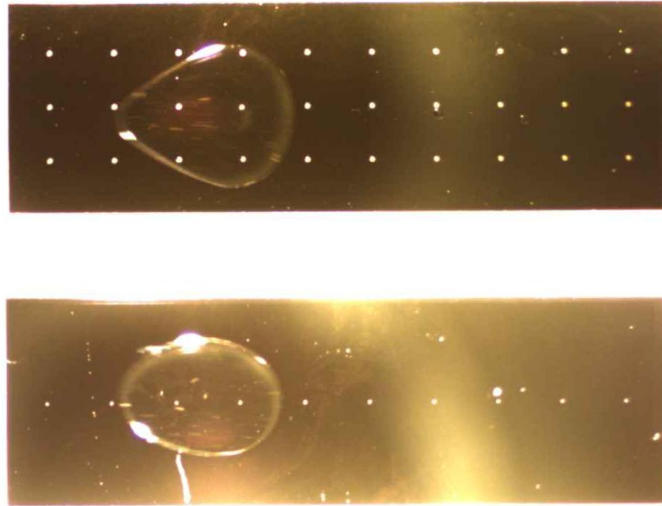


Figure 14. Photograph illustrating teardrop shape of electrolyte droplet with 3-wide site configuration. (Top) Strip 4.10 with 3-wide configuration. (Bottom) Strip 4.01 with single row configuration. In both images, droplet motion is to the right and droplet volume is 50 μl .

When ANOVA was performed on the data for droplet velocities, the results agreed with the above discussion (see Table 10). The site pattern factor has a p -value of only 0.0249, which meets the common cut-off of 0.05. This indicates that the null hypothesis can likely be rejected, showing that the site pattern has a statistically significant impact on the droplet velocity. With the other two factors the p -values were not low enough to allow us to reject the null hypothesis.

Table 10. *P*-values from ANOVA performed on droplet velocity data

Site Diameter	Site Spacing	Site Pattern
0.4582	0.2045	0.0249

In addition to trends in the quantifiable performance metrics used, there is insight to be had from more qualitative assessments. While the single-row site configuration seems to be more desirable from a velocity standpoint, strips with this configuration showed increased susceptibility to damage and unexplained failure. Degradation of the aluminum sites due to electrolysis is expected, and it would make sense that those strips with a single row of sites would be more prone to failure over time, since if a single site is degraded to the point of non-functionality, the chain of sites is broken and droplet motion will cease. The three-wide configuration has the benefit of redundancy at each step in the chain of sites, which is likely the cause of the increased durability observed. Additionally, for a given site size, a three-wide configuration will likely have reduced current densities at each site (since when the droplet is teardrop shaped, each front site is sharing the current load with 2 other sites), which should reduce the impact of aluminum etching due to electrolysis. Similar increased durability and consistency of results was noted on those strips which had a larger site diameter, which likely occurs for similar reasons as just discussed.

Chapter 5.

Conclusion

5.1 Summary

In this thesis, a new approach to achieving micro-droplet transport using electrowetting on dielectric techniques is presented. EWOD is the reduction in apparent contact angle of a fluid droplet using the capacitance of a dielectric layer which lies between the droplet and an electrode. Applying voltage across this barrier (between the droplet and electrode) causes charge migration to occur within the droplet and electrode, which modifies the apparent surface energy of the droplet, causing its contact angle to be reduced. The field of EWOD research has seen significant advancement in the previous decade. Applications for electrowetting in general are diverse, ranging from the shaping of microlenses, fiber optics switching, display technology, and optical filters to such interesting areas as the creation of small low-power-consumption motors. When looking at applications for droplet EWOD droplet transport, the most significant (with much interest and diversity of research) is in lab-on-a-chip designs. Also, the use of droplet motion to assist in assembly of nano- and micro-scale components for microdevices holds promise. In both these applications the ability to accurately control the motion of a micro-droplet, reducing the operating voltage and power

of such devices and reducing their complexity of construction and operation are of paramount concern.

A significant step in reducing complexity of the device is accomplished here by replacing the current paradigm with one of our design. Most current devices use arrays of individual electrodes to induce geometrically – asymmetric electrowetting (where only a portion of the droplet has its contact angle reduced) and hence droplet motion. This increases the complexity of the final device, as well as of the controls needed (as they require precise control of switching/timing of a large number of small electrodes). In our design, this complex array is reduced to a single electrical circuit, and the motion achieved is continuous (not in discrete steps). This is accomplished by the replacement of portions of the dielectric layer with aluminum sites, creating areas that regulate current flow between droplet and substrate in a diode-like current rectifying manner.

Aluminum and other valve metals have been known to exhibit diode-like properties in electrolytic cells, and in fact this behavior is taken advantage of in electrolytic capacitors. As a droplet covers multiple aluminum sites on a test strip, with a voltage being applied across the entire strip, the adjacent sites are at different potentials due to the resistivity of the electrode. Since aluminum-electrolyte interfaces act cathodically forward the more negatively charged site will allow current flow between electrode and droplet, while the more positively charged one will not. This impediment to current flow results in the contact angle reduction of the leading edge of the drop, causing motion in the direction of

positive voltage gradient. By patterning an array of these sites, continuous motion has been achieved.

Multiple wafers were fabricated, and the effect of the thickness of the dielectric and surface treatment layers was explored. Additionally, further testing with various electrolyte and ambient phases was conducted, which resulted in the most impressive gains in performance. Lastly, comparative testing was performed on test strips from a single wafer to explore the effect of site diameter, spacing and pattern on device performance. Testing of the various wafers produced showed that caution must be taken in reducing the thickness of the dielectric layer in an attempt to increase the specific capacitance, as the potential increases for allowing conduction across the dielectric (as seen in Wafer 2). Since the surface treatment layer contributes little in the way of dielectric properties, its thickness was safely reduced from that used in our original wafer design. The results of comparative testing of strips from Wafer 4 reveal some dependence of velocity on site configuration, while minimum actuation voltage testing indicates there may be some dependence on site spacing (which was expected) though it is difficult to make that assertion based on variability of the data.

5.2 Future Work

Many opportunities exist for future work exploring the design presented here, most centering on the goal of reducing voltage requirements and increasing

consistency and dependability of the device. One of the most obvious methods of doing so is to reduce the total thickness of the dielectric layer(s) used in order to increase the specific capacitance (and hence electrowetting response at a given voltage). While attempts were made in this area, the dielectric used (SiO_2) was not suited to the thinner layers, showing some leakage of current. The possibility exists to use atomic layer deposition (ALD) to lay down high-permittivity dielectrics (such as Al_2O_3), in very thin layers that still maintain their impermeability to current flow [45-48].

Other suggestions for minor improvements to any further testing on similar devices center on the fluids used. As noted, significant gains in device performance could be had by changing electrolyte-ambient phase system, demonstrating the strong influence these two factors have on the overall device. As such, in further testing, it should be emphasized that controlling the consistency of the depth of ambient phase used is desirable to ensure consistent results. Also, it is recommended that several other potential electrolyte fluids be tested to evaluate their performance, possibly fluids that are predicted to have common use in lab-on-a-chip testing.

Another area of study that presents itself is exploring changes to the valve metal sites. Many aspects of the site can be adjusted to explore their impact on device performance. Aluminum is only one of many valve metals, with tantalum often being mentioned in literature as one that exhibits particularly strong current rectification. Testing with tantalum sites to evaluate their diode-like behavior and

durability compared to aluminum would be insightful. Additionally, regardless of the valve metal used, varying the site dimensions (both diameter and thickness) could have an impact on site durability as well by changing the amount of material present and the current density it is exposed to. In particular it may be advisable to select site diameters that are more drastically different from each other, in an effort to make more noticeable any effect of site diameter on performance,

Another area of potential future research which would increase understanding of the principles at work in this device is to increase the accuracy of modeling. With further characterization of the diode-like behavior of the valve metal sites, it may be possible to model their behavior using a variation of the Shockley diode equation, allowing for better prediction of electrical behavior at these sites. In a similar vein, a question arose during this work as to what the electrical behavior (current and voltage) at the sites was when a droplet is covering 3 or more sites. It is clear cut with only two sites that one will be reverse biased and one forward, but the situation becomes more complex as more 'diodes' are added to the mix. A more complete understanding of this behavior would provide significant insight into possible improved designs, especially in the area of site spacing.

List of References

- [1] Mugele, F., 2005, "Electrowetting: From Basics to Applications," Journal of Physics. Condensed Matter, **17**(28) pp. R705.
- [2] Lippmann, G., 1875, "Relations Entre Les Phénomènes Électrique Et Capillaries," Annales Des Chimie Et Des Physique, **5**pp. 494.
- [3] de Gennes, P.G., Brochard Wyart, F., and Quere, D., 2004, "Capillarity and wetting phenomena ; drops, bubbles, pearls, waves," Springer-Verlag, New York, pp. 291.
- [4] Langbein, D.W., 2002, "Capillary surfaces : shape-stability-dynamics, in particular under weightlessness," Springer, Berlin ; New York, pp. 364.
- [5] Anonymous 2010, "New Compact eReader Concept Unveiled by Liquavista and GBO Design-Engineering," 2010(15 October 2010) .
- [6] Kaige, S., 2008, "Reflective display device based on electrowetting," pp. 4.
- [7] Heikenfeld, J., 2007, "Recent advances in electrowetting display fabrication, device architectures, and performance," pp. 290-293.
- [8] Kaichang, Z., 2007, "Electrowetting light valves for electronic paper," pp. 288-9.
- [9] Sun, B., 2007, "Scalable Fabrication of Electrowetting Displays with Self-Assembled Oil Dosing," Applied Physics Letters, **91**(1) pp. 011106-011106.
- [10] Berge, B., 2000, "Variable Focal Lens Controlled by an External Voltage: An Application of Electrowetting," The European Physical Journal.E, Soft Matter, **3**(2) pp. 159.
- [11] Mach, P., 2002, "Dynamic Tuning of Optical Waveguides with Electrowetting Pumps and Recirculating Fluid Channels," Applied Physics Letters, **81**(2) pp. 202.

- [12] Berg, A.v.d., and Oosterbroek, R.E., 2003, "Lab-on-a-chip : miniaturized systems for (bio)chemical analysis and synthesis," Elsevier, Amsterdam ; Boston, pp. 394.
- [13] Li, P.H., 2006, "Microfluidic lab-on-a-chip for chemical and biological analysis and discovery," Taylor & Francis/CRC Press, Boca Raton, pp. 504.
- [14] Geschke, O., Klank, H., Telleman, P., 2004, "Microsystem engineering of lab-on-a-chip devices," Wiley-VCH, Weinheim, pp. 258.
- [15] Fair, R.B., 2003, "Electrowetting-based on-chip sample processing for integrated microfluidics," pp. 32-4.
- [16] Pollack, M. G., 2002, "Electrowetting-Based Actuation of Droplets for Integrated Microfluidics," Lab on a Chip, **2**(2) pp. 96-101.
- [17] Pamula, V.K., 2002, "Microfluidic electrowetting-based droplet mixing," pp. 8-10.
- [18] Junghoon, L., 2002, "Electrowetting and Electrowetting-on-Dielectric for Microscale Liquid Handling," Sensors and Actuators.A, Physical, **95**(2) pp. 259.
- [19] Cho, S., 2003, "Creating, Transporting, Cutting, and Merging Liquid Droplets by Electrowetting-Based Actuation for Digital Microfluidic Circuits," Journal of Microelectromechanical Systems, **12**(1) pp. 70.
- [20] Mazutis, L., 2009, "A Fast and Efficient Microfluidic System for Highly Selective One-to-One Droplet Fusion," Lab on a Chip, **9**(18) pp. 2665-72.
- [21] Mugele, F., 2006, "Microfluidic Mixing through Electrowetting-Induced Droplet Oscillations," Applied Physics Letters, **88**(20) pp. 204106-1.
- [22] Sang, K., 2009, "Electrowetting Propulsion of Water-Floating Objects," Applied Physics Letters, **95**(1) pp. 014107.
- [23] Mita, Y., 2009, "Demonstration of a Wireless Driven MEMS Pond Skater that Uses EWOD Technology," Solid-State Electronics, **53**(7) pp. 798.
- [24] Takei, A., 2007, "Liquid motor driven by electrowetting," pp. 42.
- [25] Young, L., 1961, "Anodic oxide films," Academic Press, London, New York, pp. 377.

- [26] Frumkin, A., 1920, "On the Theory of Electro-Capillarity," The Philosophical Magazine, **40**pp. 363-385.
- [27] Frumkin, A., 1930, "Electrocapillary Properties of Amalgams," Journal of Physical Chemistry, **34**pp. 74-85.
- [28] Sondag-Huethorst, J., and Fokkink, L. G. J., 1994, "Potential-Dependent Wetting of Electroactive Ferrocene-Terminated Alkanethiolate Monolayers on Gold," Langmuir, **10**(11) pp. 4380-4387.
- [29] Berge, B., 1993, "Electrocapillarity and Wetting of Insulator Films by Water," Comptes Rendus De l'Académie Des Sciences.Série II, Mécanique, Physique, Chimie, Sciences De l'Univers, Sciences De La Terre, **317**(2) pp. 157.
- [30] Li, Y., 2008, "Room-Temperature Fabrication of Anodic Tantalum Pentoxide for Low-Voltage Electrowetting on Dielectric (EWOD)," Journal of Microelectromechanical Systems, **17**(6) pp. 1481.
- [31] Vermilyea, D. A., 1965, "Conduction and Rectification in Anodic Oxide Films," Journal of Applied Physics, **36**(11) pp. 3663-3671.
- [32] Vijh, A., 1977, "OXIDE AND OXIDE FILMS, VOLUME 5, 1977." .
- [33] Newbery, E., 1932, "Electrolytic Valve Action and Electrolytic Rectifiers," Proceedings of the Royal Society of London.Series A, Containing Papers of a Mathematical and Physical Character, **137**(831) pp. 134-145.
- [34] Aleksandrov, L. N., 1998, "Morphology of Porous Silicon Structures Formed by Anodization of Heavily and Lightly Doped Silicon," Thin Solid Films, **330**(2) pp. 102.
- [35] Tanaka, H., 2004, "In Situ Measurement of the Diameter of Nanopores in Silicon during Anodization in Hydrofluoric Acid Solution," Journal of the Electrochemical Society, **151**(6) pp. C439.
- [36] Crane, N., Volinsky, A., Mishra, P., 2010, "Bidirectional Electrowetting Actuation with Voltage Polarity Dependence," Applied Physics Letters, **96**(10) pp. 104103.
- [37] Card, H. C., 1976, "Aluminum—Silicon Schottky Barriers and Ohmic Contacts in Integrated Circuits," Electron Devices, IEEE Transactions on, **23**(6) pp. 538-544.

- [38] Andrews, J. M., 1974, "ROLE OF THE METAL-SEMICONDUCTOR INTERFACE IN SILICON INTEGRATED CIRCUIT TECHNOLOGY." The Journal of Vacuum Science and Technology, **11**(6) pp. 972-984.
- [39] Raj, B., 2008, "Composite dielectrics and surfactants for low voltage electrowetting devices," pp. 187-90.
- [40] Crane, N., 2008, "Analysis and measurement of forces in an electrowetting-driven oscillator," pp. 285-290.
- [41] Crane, N. B., 2010, "Characterization of Electrowetting Processes through Force Measurements," Review of Scientific Instruments Online, **81**(4) pp. 043902-043902.
- [42] Raj, B., Dhindsa, M., Smith, N. R., 2009, "Ion and Liquid Dependent Dielectric Failure in Electrowetting Systems," Langmuir, **25**(20) pp. 12387-12392.
- [43] Restolho, J., 2009, "Electrowetting of Ionic Liquids: Contact Angle Saturation and Irreversibility," Journal of Physical Chemistry, **C**(113) pp. 9321-9327.
- [44] Nanayakkara, Y., 2008, "A Fundamental Study on Electrowetting by Traditional and Multifunctional Ionic Liquids: Possible use in Electrowetting on Dielectric-Based Microfluidic Applications," Analytical Chemistry, **80**(20) pp. 7690.
- [45] Kukli, K., 2003, "Atomic layer deposition chemistry, mechanisms and related physical properties of high permittivity dielectric oxides," pp. 106-11.
- [46] Bethge, O., 2009, "Low Temperature Atomic Layer Deposition of High-k Dielectric Stacks for Scaled Metal-Oxide-Semiconductor Devices," Thin Solid Films, **517**(18) pp. 5543-7.
- [47] Ghirdelli, E., 2008, "Growth of Dielectric Al₂O₃ Films by Atomic Layer Deposition," Japanese Journal of Applied Physics, **47**(10) pp. 8174-7.
- [48] Tanner, C. M., 2007, "Electrical Performance of Al₂O₃ Gate Dielectric Films Deposited by Atomic Layer Deposition on 4H-SiC," Applied Physics Letters, **91**(20) pp. 203510-1.

Appendices

Appendix A. Modified C++ Code for Camera Trigger Software

The code which follows is from IDS Imaging as part of their Software Development Kit for their uEye series of cameras. The code was modified by the addition of what are now lines 492 through 497, and the header was modified by the addition of the include directives for iostream and sstream as well as the using directive for namespace.std (modified portions are highlighted).

```
//=====/  
/  
//  
// Copyright (C) 2004 - 2009 //  
// IDS Imaging GmbH //  
// Dimbacherstr. 6 //  
// D-74182 Obersulm-Willsbach //  
//  
// The information in this document is subject to change without //  
// notice and should not be construed as a commitment by IDS Imaging GmbH. //  
// IDS Imaging GmbH does not assume any responsibility for any errors //  
// that may appear in this document. //  
//  
// This document, or source code, is provided solely as an example //  
// of how to utilize IDS software libraries in a sample application. //  
// IDS Imaging GmbH does not assume any responsibility for the use or //  
// reliability of any portion of this document or the described software. //  
//  
// General permission to copy or modify, but not for profit, is hereby //  
// granted, provided that the above copyright notice is included and //  
// reference made to the fact that reproduction privileges were granted //  
// by IDS Imaging GmbH. //  
//  
// IDS cannot assume any responsibility for the use or misuse of any //  
// portion of this software for other than its intended diagnostic purpose //  
// in calibrating and testing IDS manufactured cameras and software. //  
//  
//=====/  
/  
#include "stdafx.h"  
#include "uEyeSimpleTrigger.h"
```


Appendix A (Continued)

```
#include "uEyeSimpleTriggerDlg.h"
#include "..\uEyesimpletriggerdlg.h"
#include <iostream>
#include <sstream>

using namespace std;

extern CuEyeSimpleTriggerApp theApp;

#ifdef _DEBUG
#define new DEBUG_NEW
#undef THIS_FILE
static char THIS_FILE[] = __FILE__;
#endif

class CAboutDlg : public CDialog
{
public:
    CAboutDlg();

    enum { IDD = IDD_ABOUTBOX };

private:
    virtual void DoDataExchange(CDataExchange* pDX);

    DECLARE_MESSAGE_MAP()
};

CAboutDlg::CAboutDlg() : CDialog(CAboutDlg::IDD)
{
}

void CAboutDlg::DoDataExchange(CDataExchange* pDX)
{
    CDialog::DoDataExchange(pDX);
}

BEGIN_MESSAGE_MAP(CAboutDlg, CDialog)
END_MESSAGE_MAP()

////////////////////////////////////
CuEyeSimpleTriggerDlg::CuEyeSimpleTriggerDlg(CWnd* pParent /*=NULL*/)
    : CDialog(CuEyeSimpleTriggerDlg::IDD, pParent)
{
    m_hIcon = AfxGetApp()->LoadIcon(IDR_MAINFRAME);
}

```

Appendix A (Continued)

```
void CuEyeSimpleTriggerDlg::DoDataExchange(CDataExchange* pDX)
{
    CDialog::DoDataExchange(pDX);
    DDX_Radio(pDX, IDC_RADIO_OFF, m_nTriggerMode);
    DDX_Text(pDX, IDC_EDIT_FRAME_EVENTS, m_nFrameEvents);
    DDX_Text(pDX, IDC_EDIT_TRIGGER_EVENTS, m_nTriggerEvents);
}

BEGIN_MESSAGE_MAP(CuEyeSimpleTriggerDlg, CDialog)
    ON_WM_SYSCOMMAND()
    ON_WM_PAINT()
    ON_WM_QUERYDRAGICON()
    ON_BN_CLICKED(IDC_BUTTON_START, OnButtonStart)
    ON_BN_CLICKED(IDC_BUTTON_STOP, OnButtonStop)
    ON_BN_CLICKED(IDC_BUTTON_EXIT, OnButtonExit)
    ON_MESSAGE(IS_UEYE_MESSAGE, OnUEyeMessage)
    ON_BN_CLICKED(IDC_BUTTON_LOAD_PARAMETER,
OnBnClickedButtonLoadParameter)
    ON_WM_CLOSE()
    ON_BN_CLICKED(IDC_RADIO_OFF, OnBnClickedRadioTrigger)
    ON_BN_CLICKED(IDC_RADIO_SOFTWARE, OnBnClickedRadioTrigger)
    ON_BN_CLICKED(IDC_RADIO_LO_HI, OnBnClickedRadioTrigger)
    ON_BN_CLICKED(IDC_RADIO_HI_LO, OnBnClickedRadioTrigger)
    ON_BN_CLICKED(IDC_BUTTON_RESET_COUNTERS, OnBnClickedButtonResetCounters)
END_MESSAGE_MAP()

////////////////////////////////////
BOOL CuEyeSimpleTriggerDlg::OnInitDialog()
{
    CDialog::OnInitDialog();

    ASSERT((IDM_ABOUTBOX & 0xFFF0) == IDM_ABOUTBOX);
    ASSERT(IDM_ABOUTBOX < 0xF000);

    CMenu* pSysMenu = GetSystemMenu(FALSE);
    if (pSysMenu != NULL)
    {
        CString strAboutMenu;
        strAboutMenu.LoadString(IDS_ABOUTBOX);
        if (!strAboutMenu.IsEmpty())
        {
            pSysMenu->AppendMenu(MF_SEPARATOR);
            pSysMenu->AppendMenu(MF_STRING, IDM_ABOUTBOX, strAboutMenu);
        }
    }

    // Will only be enabled if in stop mode
    GetDlgItem(IDC_BUTTON_LOAD_PARAMETER)->EnableWindow(FALSE);
}
```

Appendix A (Continued)

```
// Set the icon for this dialog. The framework does this automatically
// when the application's main window is not a dialog
SetIcon(m_hIcon, TRUE);           // Set big icon
SetIcon(m_hIcon, FALSE);        // Set small icon

// Get handle to display window
m_hWndDisplay = GetDlgItem( IDC_DISPLAY )->m_hWnd;

m_pcImageMemory = NULL;
m_lMemoryId = 0;
m_hCam = 0;
m_nRenderMode = IS_RENDER_FIT_TO_WINDOW;
m_nPosX = 0;
m_nPosY = 0;
m_nFlipHor = 0;
m_nFlipVert = 0;

m_nTriggerMode = 0;
m_nFrameEvents = 0;
m_nTriggerEvents = 0;

UpdateData(FALSE);

// Open a camera
OpenCamera();

// Deactivate button "Start"
GetDlgItem(IDC_BUTTON_START)->EnableWindow(FALSE);

return true;
}

void CuEyeSimpleTriggerDlg::OnSysCommand(UINT nID, LPARAM lParam)
{
    if ((nID & 0xFFF0) == IDM_ABOUTBOX)
    {
        CAboutDlg dlgAbout;
        dlgAbout.DoModal();
    }
    else
    {
        CDialog::OnSysCommand(nID, lParam);
    }
}

void CuEyeSimpleTriggerDlg::OnPaint()
{
```

Appendix A (Continued)

```
    if (IsIconic())
    {
        CPaintDC dc(this); // device context for painting

        SendMessage(WM_ICONERASEBKGND, (WPARAM) dc.GetSafeHdc(), 0);

        // Center icon in client rectangle
        int cxIcon = GetSystemMetrics(SM_CXICON);
        int cyIcon = GetSystemMetrics(SM_CYICON);
        CRect rect;
        GetClientRect(&rect);
        int x = (rect.Width() - cxIcon + 1) / 2;
        int y = (rect.Height() - cyIcon + 1) / 2;

        // Draw the icon
        dc.DrawIcon(x, y, m_hIcon);
    }
    else
    {
        CDialog::OnPaint();
    }
}

// The system calls this to obtain the cursor to display while the user drags
// the minimized window.
HCURSOR CuEyeSimpleTriggerDlg::OnQueryDragIcon()
{
    return (HCURSOR) m_hIcon;
}

/////////////////////////////////////////////////////////////////
//
// METHOD OnButtonStart()
//
// DESCRIPTION: start capture and return immediately
//
/////////////////////////////////////////////////////////////////
void CuEyeSimpleTriggerDlg::OnButtonStart()
{
    if( m_hCam == 0 )
    {
        OpenCamera();
    }

    if( m_hCam != 0 )
    {
        // Capture video (live or trigger)
        is_CaptureVideo( m_hCam, IS_DONT_WAIT );
    }
}
```

Appendix A (Continued)

```
        /*is_CaptureVideo( m_hCam, IS_WAIT );*/

        // Disable button 'Load Parameters'
        GetDlgItem(IDC_BUTTON_LOAD_PARAMETER)->EnableWindow(FALSE);

        m_bLive = TRUE;

        // Deactivate button "Start"
        GetDlgItem(IDC_BUTTON_START)->EnableWindow(FALSE);

        // Activate button "Stop"
        GetDlgItem(IDC_BUTTON_STOP)->EnableWindow(TRUE);
    }
}

/////////////////////////////////////////////////////////////////
//
// METHOD OnButtonStop()
//
// DESCRIPTION: stop capture and return immediately
//
/////////////////////////////////////////////////////////////////
void CuEyeSimpleTriggerDlg::OnButtonStop()
{
    // Stop immediately - force stop
    if( m_hCam != 0 )
    {
        is_StopLiveVideo( m_hCam, IS_FORCE_VIDEO_STOP );

        m_bLive = FALSE;

        // Activate button "Start"
        GetDlgItem(IDC_BUTTON_START)->EnableWindow(TRUE);

        // Deactivate button "Stop"
        GetDlgItem(IDC_BUTTON_STOP)->EnableWindow(FALSE);
    }

    // Enable button 'Load Parameters'
    GetDlgItem(IDC_BUTTON_LOAD_PARAMETER)->EnableWindow(TRUE);
}

/////////////////////////////////////////////////////////////////
//
// METHOD OnBnClickedButtonResetCounters()
//
// DESCRIPTION: reset the frame and trigger counters
//
```

Appendix A (Continued)

```
////////////////////////////////////
void CuEyeSimpleTriggerDlg::OnBnClickedButtonResetCounters()
{
    // Reset the counters
    m_nFrameEvents = 0;
    m_nTriggerEvents = 0;

    UpdateData(FALSE);
}

////////////////////////////////////
//
// METHOD OnBnClickedButtonLoadParameter()
//
// DESCRIPTION: - loads parameters from an ini file
//               - reallocates the memory
//
////////////////////////////////////
void CuEyeSimpleTriggerDlg::OnBnClickedButtonLoadParameter()
{
    if ( m_hCam == 0 )
    {
        OpenCamera();
    }

    if ( m_hCam != 0 )
    {
        if( is_LoadParameters( m_hCam, NULL ) == IS_SUCCESS && m_pcImageMemory != NULL )
        {
            // Determine live capture
            BOOL bWasLive = (BOOL)(is_CaptureVideo( m_hCam, IS_GET_LIVE ));
            if( bWasLive )
            {
                is_StopLiveVideo(m_hCam, IS_FORCE_VIDEO_STOP);
            }

            // Realloc image mem with actual sizes and depth.
            is_FreeImageMem( m_hCam, m_pcImageMemory, m_lMemoryId );
            m_nSizeX = is_SetImageSize( m_hCam, IS_GET_IMAGE_SIZE_X, 0 );
            m_nSizeY = is_SetImageSize( m_hCam, IS_GET_IMAGE_SIZE_Y, 0 );

            switch( is_SetColorMode( m_hCam, IS_GET_COLOR_MODE ) )
            {
                case IS_SET_CM_RGB32:
                    m_nBitsPerPixel = 32;
                    break;

                case IS_SET_CM_RGB24:
                    m_nBitsPerPixel = 24;
            }
        }
    }
}
```

Appendix A (Continued)

```
        break;

    case IS_SET_CM_RGB16:
    case IS_SET_CM_UYVY:
        m_nBitsPerPixel = 16;
        break;

    case IS_SET_CM_RGB15:
        m_nBitsPerPixel = 15;
        break;

    case IS_SET_CM_Y8:
    case IS_SET_CM_RGB8:
    case IS_SET_CM_BAYER:
    default:
        m_nBitsPerPixel = 8;
        break;
    }

    // Memory initialization
    is_AllocImageMem( m_hCam, m_nSizeX, m_nSizeY, m_nBitsPerPixel, &m_pcImageMemory,
&m_lMemoryId);

    // Set memory active
    is_SetImageMem(m_hCam, m_pcImageMemory, m_lMemoryId );

    // Display initialization
    is_SetImageSize(m_hCam, m_nSizeX, m_nSizeY );

    // Run live again
    if( bWasLive )
    {
        is_CaptureVideo(m_hCam, IS_DONT_WAIT);
    }
}
}
}

/////////////////////////////////////////////////////////////////
//
// METHOD OnButtonExit()
//
// DESCRIPTION: - stop capture
//               - free used image memory
//               - exit the camera
//               - quit application
//
/////////////////////////////////////////////////////////////////
void CuEyeSimpleTriggerDlg::OnButtonExit()
```

Appendix A (Continued)

```
{
    ExitCamera();
    PostQuitMessage( 0 );
}

/////////////////////////////////////////////////////////////////
//
// METHOD OpenCamera()
//
// DESCRIPTION: - Opens a handle to a connected camera
//
/////////////////////////////////////////////////////////////////
bool CuEyeSimpleTriggerDlg::OpenCamera()
{
    INT nRet = IS_NO_SUCCESS;
    ExitCamera();

    // Init camera (open next available camera)
    m_hCam = (HIDS) 0;
    nRet = InitCamera(&m_hCam, m_hWndDisplay);
    if (nRet == IS_SUCCESS)
    {
        // Retrieve original image size
        is_GetSensorInfo(m_hCam, &m_sInfo);
        m_nSizeX = m_sInfo.nMaxWidth;
        m_nSizeY = m_sInfo.nMaxHeight;

        UpdateData(TRUE);
        nRet = InitDisplayMode();

        if (nRet == IS_SUCCESS)
        {
            // Enable Messages
            is_EnableMessage(m_hCam, IS_DEVICE_REMOVED, GetSafeHwnd());
            is_EnableMessage(m_hCam, IS_DEVICE_RECONNECTED, GetSafeHwnd());
            is_EnableMessage(m_hCam, IS_FRAME, GetSafeHwnd());
            is_EnableMessage(m_hCam, IS_TRIGGER, GetSafeHwnd());

            // Start capture
            if(is_CaptureVideo( m_hCam, IS_WAIT ) == IS_SUCCESS)
            {
                m_bLive = TRUE;
            }
        }
        else
        {
            AfxMessageBox(TEXT("Initializing the display mode failed!"),
                MB_ICONWARNING );
        }
    }
}
```


Appendix A (Continued)

```
        return true;
    }
    else
    {
        AfxMessageBox(TEXT("No uEye camera could be opened !"), MB_ICONWARNING );
        return false;
    }
}
```

```
////////////////////////////////////
//
// METHOD OnUEyeMessage()
//
// DESCRIPTION: - handles the messages from the uEye camera
//               - messages must be enabled using is_EnableMessage()
//
////////////////////////////////////
LRESULT CuEyeSimpleTriggerDlg::OnUEyeMessage( WPARAM wParam, LPARAM lParam )
{
    UpdateData(FALSE);

    switch ( wParam )
    {
        case IS_DEVICE_REMOVED:
            Beep( 400, 50 );
            break;

        case IS_DEVICE_RECONNECTED:
            Beep( 400, 50 );
            break;

        case IS_FRAME:
            if( m_pcImageMemory != NULL )
            {
                m_nFrameEvents++;
                is_RenderBitmap( m_hCam, m_lMemoryId, m_hWndDisplay, m_nRenderMode );
            }
            break;

        case IS_TRIGGER:
            m_nTriggerEvents++;
            stringstream ss (stringstream::in | stringstream::out);
            ss<< m_nTriggerEvents;
            string fileindex = ss.str();
            string filename = "C:\\Documents and Settings\\cmlynch2\\My
Documents\\uEye Triggered Images\\" + fileindex + ".jpg";
            const char* filechar = filename.c_str();
            is_SaveImageEx(m_hCam, filechar, IS_IMG_JPG, 40);
    }
}
```

Appendix A (Continued)

```
        break;
    }
    return 0;
}

/////////////////////////////////////////////////////////////////
//
// METHOD ExitCamera()
//
// DESCRIPTION: - exits the instance of the camera
//
/////////////////////////////////////////////////////////////////
void CuEyeSimpleTriggerDlg::ExitCamera()
{
    if( m_hCam != 0 )
    {
        // Disable messages
        is_EnableMessage(m_hCam, IS_DEVICE_REMOVED, NULL);
        is_EnableMessage(m_hCam, IS_DEVICE_RECONNECTED, NULL);
        is_EnableMessage(m_hCam, IS_FRAME, NULL);
        is_EnableMessage(m_hCam, IS_TRIGGER, NULL);

        // Stop live video
        is_StopLiveVideo( m_hCam, IS_WAIT );

        // Free the allocated buffer
        if( m_pcImageMemory != NULL )
        {
            is_FreeImageMem( m_hCam, m_pcImageMemory, m_lMemoryId );
        }

        m_pcImageMemory = NULL;

        // Close camera
        is_ExitCamera( m_hCam );
        m_hCam = NULL;
    }
}

/////////////////////////////////////////////////////////////////
//
// METHOD InitDisplayMode()
//
// DESCRIPTION: - initializes the display mode
//
/////////////////////////////////////////////////////////////////
int CuEyeSimpleTriggerDlg::InitDisplayMode()
{
    INT nRet = IS_NO_SUCCESS;
}
```

Appendix A (Continued)

```
if (m_hCam == NULL)
{
    return IS_NO_SUCCESS;
}

if( m_pcImageMemory != NULL )
{
    is_FreeImageMem( m_hCam, m_pcImageMemory, m_lMemoryId );
}
m_pcImageMemory = NULL;

// Set display mode to DIB
nRet = is_SetDisplayMode(m_hCam, IS_SET_DM_DIB);
if (m_sInfo.nColorMode == IS_COLORMODE_BAYER)
{
    // Setup the color depth to the current windows setting
    is_GetColorDepth(m_hCam, &m_nBitsPerPixel, &m_nColorMode);
}
else
{
    // For monochrome camera models use Y8 mode
    m_nColorMode = IS_SET_CM_Y8;
    m_nBitsPerPixel = 8;
}

// Allocate an image memory.
if (is_AllocImageMem(m_hCam, m_nSizeX, m_nSizeY, m_nBitsPerPixel, &m_pcImageMemory,
&m_lMemoryId ) != IS_SUCCESS)
{
    AfxMessageBox(TEXT("Memory allocation failed!"), MB_ICONWARNING );
}
else
{
    is_SetImageMem( m_hCam, m_pcImageMemory, m_lMemoryId );
}

if (nRet == IS_SUCCESS)
{
    // Set the desired color mode
    is_SetColorMode(m_hCam, m_nColorMode);

    // Set the image size to capture
    is_SetImageSize(m_hCam, m_nSizeX, m_nSizeY);
}

return nRet;
}
```

Appendix A (Continued)

```
void CuEyeSimpleTriggerDlg::OnClose()
{
    ExitCamera();
    CDialog::OnClose();
}

/////////////////////////////////////////////////////////////////
//
// METHOD OnBnClickedRadioTrigger()
//
// DESCRIPTION: - deactivates or changes the trigger mode
//
/////////////////////////////////////////////////////////////////
void CuEyeSimpleTriggerDlg::OnBnClickedRadioTrigger()
{
    if (!UpdateData(TRUE))
    {
        return;
    }

    if(m_bLive == TRUE)
    {
        is_StopLiveVideo(m_hCam, IS_WAIT);
    }

    // Trigger off
    if(m_nTriggerMode == 0)
    {
        is_SetExternalTrigger(m_hCam, IS_SET_TRIG_OFF);
    }
    // Software trigger
    if(m_nTriggerMode == 1)
    {
        is_SetExternalTrigger(m_hCam, IS_SET_TRIGGER_SOFTWARE);
    }
    // Hardware trigger falling edge
    else if(m_nTriggerMode == 2)
    {
        is_SetExternalTrigger(m_hCam, IS_SET_TRIGGER_HI_LO);
    }
    // Hardware trigger rising edge
    else if(m_nTriggerMode == 3)
    {
        is_SetExternalTrigger(m_hCam, IS_SET_TRIGGER_LO_HI);
    }

    if(m_bLive == TRUE)
    {
        is_CaptureVideo(m_hCam, IS_DONT_WAIT);
    }
}
```

Appendix A (Continued)

```
    }
}

INT CuEyeSimpleTriggerDlg::InitCamera (HIDS *hCam, HWND hWnd)
{
    INT nRet = is_InitCamera (hCam, hWnd);

    /*****
    *****/
    /*
    /*
    /* If the camera returns with "IS_STARTER_FW_UPLOAD_NEEDED", an upload of a new firmware
    /*
    /* is necessary. This upload can take several seconds. We recommend to check the required
    /* time with the function is_GetDuration().
    /*
    /* In this case, the camera can only be opened if the flag "IS_ALLOW_STARTER_FW_UPLOAD"
    /*
    /* is "OR"-ed to m_hCam. This flag allows an automatic upload of the firmware.
    /*
    /*
    /*****
    *****/
    if (nRet == IS_STARTER_FW_UPLOAD_NEEDED)
    {
        // Time for the firmware upload = 25 seconds by default
        INT nUploadTime = 25000;
        is_GetDuration (NULL, IS_SE_STARTER_FW_UPLOAD, &nUploadTime);

        CString Str1, Str2, Str3;
        Str1 = "This camera requires a new firmware. The upload will take about";
        Str2 = "seconds. Please wait ...";
        Str3.Format ("%s %d %s", Str1, nUploadTime / 1000, Str2);
        AfxMessageBox (Str3, MB_ICONWARNING);

        // Set mouse to hourglass
        SetCursor(AfxGetApp()->LoadStandardCursor(IDC_WAIT));

        // Try again to open the camera. This time we allow the automatic upload of the firmware by
        // specifying "IS_ALLOW_STARTER_FIRMWARE_UPLOAD"
        *hCam = (HIDS) (((INT)*hCam) | IS_ALLOW_STARTER_FW_UPLOAD);
        nRet = is_InitCamera (hCam, hWnd);
    }

    return nRet;
}
```